Marine Chemistry 115 (2009) 176–195

Contents lists available at ScienceDirect

Marine Chemistry

journal homepage: www.elsevier.com/locate/marchem

Dissolved aluminium and the silicon cycle in the Arctic Ocean

R. Middag [a,*], H.J.W. de Baar [a,b], P. Laan [a], K. Bakker [a]

[a] Royal Netherlands Institute for Sea Research (Royal NIOZ), P.O. BOX 59, 1790 AB Den Burg, Texel, The Netherlands
[b] Department of Ocean Ecosystems, University of Groningen, Groningen, The Netherlands

ARTICLE INFO

Article history:
Received 11 November 2008
Received in revised form 8 July 2009
Accepted 17 August 2009
Available online 24 August 2009

Keywords:
Aluminium
Silicon
Arctic Ocean
Trace metals
Distributions
Geotraces

ABSTRACT

Concentrations of dissolved (0.2 µm filtered) aluminium (Al) have been determined for the first time in the Eurasian part of the Arctic Ocean over the entire water column during expedition ARK XXII/2 aboard R.V. Polarstern (2007). An unprecedented number of 666 samples was analysed for 44 stations along 5 ocean transects. Dissolved Al in surface layer water (SLW) was very low, close to 1 nM, with lowest SLW concentrations towards the Canadian part of the Arctic Ocean and higher values adjacent to and in the shelf seas. The low SLW concentrations indicate no or little influence from aeolian dust input. Dissolved Al showed a nutrient-type increase with depth up to 28 nM, but large differences existed between the different deep Arctic basins. The differences in concentrations of Al between water masses and basins could largely be related to the different origins of the water masses. In the SLW and intermediate water layers, Atlantic and Pacific inflows were of importance. Deep shelf convection appeared to influence the Al distribution in the deep Eurasian Basin. The Al distribution of the deep Makarov Basin provides evidence for Eurasian Basin water inflow into the deep Makarov Basin. A strong correlation between Al and Silicon (Si) was observed in all basins. This correlation and the nutrient-like profile indicate a strong biological influence on the cycling and distribution of Al. The biological influence can be direct by the incorporation of Al in biogenic silica, indirect by preferential scavenging of Al onto biogenic siliceous particles, or by a combination of both processes. From the slope of the overall Al–Si relationship in the intermediate water layer (AIDW; ~200–2000 m depth), an Al/Si ratio of 2.2 atoms Al per 1000 atoms Si was derived. This ratio is consistent with the range of previously reported Al/Si uptake ratio in biogenic opal frustules of diatoms. In the deepest waters (>2000 m depth) a steeper slope of the Al–Si relationship of 7.4 to 13 atoms Al per 1000 atoms Si likely results from entrainment of cold shelf water into the deep basins, carrying the signal of dissolution of terrigenous particles with a much higher Al:Si ratio of crustal abundance. Only a small enrichment with such crustal Al and Si component may readily account for the higher Al:Si slope in the deepest waters.

1. Introduction

Aluminium (Al) is, with an average of 8.4% by weight, the third most abundant element in the earth's crust (Taylor, 1964), after Silicon (Si) with an average of 27% crustal abundance by weight. There is wide variability in crustal composition, nevertheless these averages when expressed as atoms imply that for each one Al atom there are about three Si atoms in the crust of the earth. Yet in seawater Al only exists in nanomolar concentrations, some two to three orders of magnitude below the micromolar concentrations of Si in seawater.

Fluvial input has initially been proposed as a major source of Al to the oceans (e.g. Stoffyn and Mackenzie 1982), yet since then it has been shown that fluvial inputs of Al to the open ocean are negligible due to estuarine removal processes (Mackin and Aller 1984; Tria et al., 2007 and references therein). Maring and Duce (1987) concluded that aeolian dust was most likely the main source of Al to the open ocean which since then has been shown convincingly (Tria et al., 2007 and references therein). Therefore, the surface concentrations of Al in remote oceans are predominantly influenced by aeolian dust deposition. Conversely in regions without significant dust deposition, the concentrations of Al are known to be below 1 nM in surface waters (Orians and Bruland, 1985; Measures and Vink, 2000; Kramer et al., 2004). The distribution of Al in ocean surface waters has been used as a tracer for atmospheric dust input, both in the field and in models (Measures and Vink, 2000; Gehlen et al., 2003; Kramer et al., 2004; Han et al., 2008). In regions with perennial sea-ice cover, like the Arctic Ocean, direct dust deposition is likely to be highly variable in place and time. When the ice melts large pulses of trace metals into the surface waters can be expected, especially when sediment material has been entrained in the ice (Measures, 1999).

The residence time of Al in surface waters is deemed to be short, from only 4 weeks to 4 years (Orians and Bruland, 1986) due to removal from the water column. Removal can be either passive or active. Passive removal has been suggested via adsorption onto

* Corresponding author. Tel.: +31 222 369 464.
E-mail address: rob.middag@nioz.nl (R. Middag).

0304-4203/$ – see front matter © 2009 Elsevier B.V. All rights reserved.
doi:10.1016/j.marchem.2009.08.002

particle surfaces (Hydes, 1983; Orians and Bruland, 1985). Indications for active uptake have been found in nutrient-like distributions of Al in the water column in some, but by no means all, ocean regions. The nutrient-like vertical profiles may indicate biological uptake of Al (Chou and Wollast, 1997; Hydes et al., 1988; Kramer et al., 2004; Stoffyn, 1979). Moreover, Gehlen et al. (2002) found that Al is structurally associated with biogenic silica due to incorporation of Al in the siliceous frustules of living diatoms in the photic surface layer. This is consistent with earlier studies of Al incorporation in opal frustules of diatoms (Van Bennekom et al., 1989, 1991; Van Beusekom and Weber, 1992). When the biogenic silica sinks out of the photic zone, it is degraded and dissolves throughout the water column, releasing the incorporated Al as well. This implies that the oceanic Al cycle is, at least partly, linked to the cycle of silicon (Si). However, not all dissolved Al and Si in the water column originate from biogenic silica as there are also contributions of terrestrial alumino-silicates via the atmosphere, sea ice, rivers and sediment interactions. These alumino-silicates originate from the continental crust and have a much higher Al/Si ratio of about 1:3 (Taylor, 1964; Wedepohl, 1995) than the average ratio of about 1:400 observed in biogenic silica (Gehlen et al., 2002 and references therein). In contrast to Al, for which the main input is believed to be via aeolian dust, Si is mainly brought into the oceans by rivers (Broecker and Peng, 1982). In the deep ocean the concentrations of Al have been suggested to be semi-conservative (Measures and Edmond, 1990) due to less scavenging removal and deep water residence times have been estimated to be between 50 and 200 years (Orians and Bruland, 1985, 1986). On the other hand, additional input of Al in the deeper water column has been suggested via diffusion from the sediments (Hydes, 1977) and pressure-dependent solubility of Al-containing particles (Moore and Millward, 1984).

The Arctic Ocean is a significant source of North Atlantic Deep Water (Rudels et al., 2000), but it is one of the least studied oceans and virtually no data, let alone reliable data, are available on the distributions and biogeochemical cycles of trace metals. Here are presented the distributions of dissolved Al in the Arctic Ocean determined during expedition ARK XXII/2 aboard R.V. Polarstern in 2007. This expedition was part of the International Polar Year — Geotraces program. Geotraces (www.geotraces.org) aims to: 'identify processes and quantify fluxes that control the distributions of key trace elements and isotopes in the ocean, and to establish the sensitivity of these distributions to changing environmental conditions' (Geotraces Science Plan, 2006). The distributions of dissolved Al are compared with the distributions of other variables, notably the concentration of silicate, the salinity and the potential temperature, in an effort to gain insight in the sources and cycling of Al in the Arctic Ocean.

2. Methods

2.1. Cleaning

The low density polyethylene bottles (LDPE, Nalgene; volumes 125, 500 and 1000 mL) used for the storage of reagents and samples were cleaned according to an intensive three step cleaning procedure. As a first step the bottles were rinsed with demineralised water, filled with a 5% concentrated detergent solution (Micro-90 diluted with demineralised water, International Products Corporation) and soaked in a 60 °C water bath for 24 h. Thereafter, the bottles were rinsed with demineralised water until visible soap residue was washed away and subsequently rinsed twice with MQ (Millipore Milli-Q deionised water $R > 18.2\ M\Omega\ cm^{-1}$). In the second step the bottles were filled with 6 M HCl (dilution with MQ from 37% HCl, reagent grade, J.T. Baker) and stored in a 60 °C water bath for 24 h. After rinsing 3 times with MQ, as the third step, the bottles were filled with 3 M HNO_3 (dilution from 65%, reagent grade, J.T. Baker) and stored 24 h in a 60 °C water bath. Finally the bottles were filled with MQ and acidified by adding 20 mL of 3 times quartz distilled 6 M HNO_3 (distilled from 65% reagent grade, J.T. Baker) per L. For transportation and storage all bottles were packed in two LDPE plastic bags. All rinsing with MQ and filling with the different acid solutions were done in a clean environment (class 100 clean room).

2.2. Sampling and filtration

Samples were taken using 24 internally Teflon-coated PVC 12 L GO-FLO samplers (General Oceanics Inc.) mounted on an all-titanium frame. This frame was connected to a 17.7 mm diameter Kevlar hydrowire with seven independent internal signal/conductor cables (Cousin Trestec S.A.) and controlled from onboard (De Baar et al., 2008). Each GO-FLO sampler had a special ultraclean all-teflon PTFE valve (Cole Parmer; PN A-06392-31) installed. Immediately upon recovery, the complete titanium frame with its 24 GO-FLO samplers was placed inside a class 100 clean room. Within this class 100 clean room environment the sub-samples for trace metal analysis were collected from the GO-FLO samplers. The water was filtered over a 0.2 μm filter cartridge (Sartobran-300, Sartorius) under pressure (1.5 atm) of (inline prefiltered) nitrogen gas exerted via a special connector instead of the regular air bleeding valve at the top of each GO-FLO sampler. Therefore, all data reported in this paper are dissolved Al. When Al is mentioned below, this implies dissolved Al. Sub-samples for Al were taken in cleaned (see above *subsection* 2.1.) LDPE sample bottles (125 mL) from each GO-FLO bottle. All sample bottles were rinsed five times with the sample seawater.

Samples for nutrients were unfiltered and collected from the GO-FLO bottles in high density poly ethylene (HDPE) sample bottles which were rinsed three times with sample water. Samples were stored in the dark at 4° prior to analysis (see *subsection* 2.5.).

2.3. Analysis of dissolved aluminium

Analyses of dissolved Al were based on a method modified after the original method developed by Resing and Measures (1994). Samples were stored in a refrigerator (4 °C) and analysed usually within 24 h after sampling but always within 36 h. Samples were acidified at least 1 h before analyses with 12 M ultraclean HCl (Baseline® Hydrochloric Acid, Seastar Chemicals Inc.) to a pH of 1.8. In a flow injection system the samples were buffered inline to a pH of 4.8 ± 0.1 with ultraclean 0.6 M ammonium acetate buffer. This buffer was produced after Aguilar-Islas et al. (2006) by diluting a saturated solution of ammonium acetate crystals to a 0.6 M solution with MQ. The pH was subsequently adjusted to 6.7 with ultraclean ammonium hydroxide. This was produced by bubbling 0.2 μm filtered high purity ammonia gas through MQ water.

The buffered sample was pre-concentrated for 240 s on a Toyopearl AF-Chelate 650 M (TosoHaas, Germany) column. Hereafter the column was rinsed for 60 s with MQ water to remove interfering salts. The Al was subsequently eluted from the column with 0.16 M HCl (Suprapure, Merck) during 250 s. The eluate of Al in HCl entered the reaction stream which consisted of a lumogallion (Pfaltz & Bauer) solution in 4 M ammonium acetate buffer. The 4 M buffer was produced similar to the 0.6 M buffer (see above), but with the pH adjusted to 6.8 ± 0.1 and the lumogallion was a 4.8 mM solution in MQ. The mixing of the HCl and buffer results in a reaction pH of 5.7 ± 0.1 at which an Al–lumogallion chelate complex is formed which can be detected by its fluorescence. The complex was mixed in a 10 m reaction coil placed in a water bath of 50 °C. Hereafter a 2.5% Brij-35 (Merck) solution in MQ was added to increase the sensitivity (Resing and Measures, 1994) and mixed in a 3 m mixing coil. Afterwards the emission of the fluorescent complex was detected on a FIA-lab PMT-FL detector with a 510 until 580 nm emission filter and a 480 until 490 nm excitation filter. Concentrations of Al were calculated in $nanomol \cdot L^{-1}$ from the peak heights (see *subsection* 2.4. below).

Table 1
Concentrations Al of surface (S) and deep (D2) SAFe samples in nM.

This work			UCSC		
Sample	Concentration Al (nM)	St dev	Sample	Concentration Al (nM)	St dev
SAFe S #252	1.76	0.05	SAFe S #57	1.64	0.08
SAFe S #252	1.75	0.05	SAFe S #214	1.68	0.06
SAFe S #425	1.65	0.05	SAFe S #574	1.68	0.07
			SAFe D2 #543	1.00	0.11
SAFe D2 #3	1.01	0.07	SAFe D2 #545	1.00	0.12
			SAFe D2 #549	0.97	0.11

Values from this work are triplicate analysis. Values from the University of California Santa Cruz (UCSC) are of 5 separate analyses per bottle for S and 4 analyses per bottle for D2 reported by Brown and Bruland (2008).

2.4. Calibration

The system was calibrated using standard additions from a 5000 nM Al stock solution (Fluka) to filtered acidified seawater of low Al concentration that was collected in the Arctic Ocean. A six-point calibration line (0, 1, 2, 4, 8 and 16 nM standard additions) and blank determination were made every day. The 3 lowest points (0, 1 and 2 nM) of the calibration line were measured in triplicate and the 3 highest points (4, 8 and 16 nM) in duplicate in order to add more weight to the lower part of the calibration line. The blank was determined by plotting the signals of increasing preconcentration times (30, 60, 120, 210 and 300 s) of the water also used for the calibration. A line was fitted through these data points and the intercept of the line taken as the blank, which was usually below 0.2 nM. If the blank was greater than 0.2 nM, the analysis run was stopped. Subsequently the system was cleaned and the blank reanalysed with freshly made sampling buffer until the blank value was below the 0.2 nM limit. The limit of detection, defined as three times the standard deviation of the lowest concentration observed, was 0.15 nM. The FIA system was cleaned every day by rinsing with a 0.5 M HCl solution.

A standard was measured in triplicate every day. This standard was a sub-sample of a 25 L volume of filtered seawater that was taken at the beginning of the expedition in the Barents Sea. The relative standard deviation of the replicate analysis seawater sample that was analysed 27 times on different days in triplicate was 3.19%. The relative standard deviation on single days was on average 2%. The average concentration of Al of this standard was 4.93 nM and the deviation from this average for a given measuring day was used as a correction factor. To verify whether this was decreasing the inter-daily variability in the dataset, every day a sample which was collected and measured the previous measuring day, was analysed once again. The deviation between the concentrations measured on the different days decreased from 3.6% to 2.8%, indicating the data correction is beneficial.

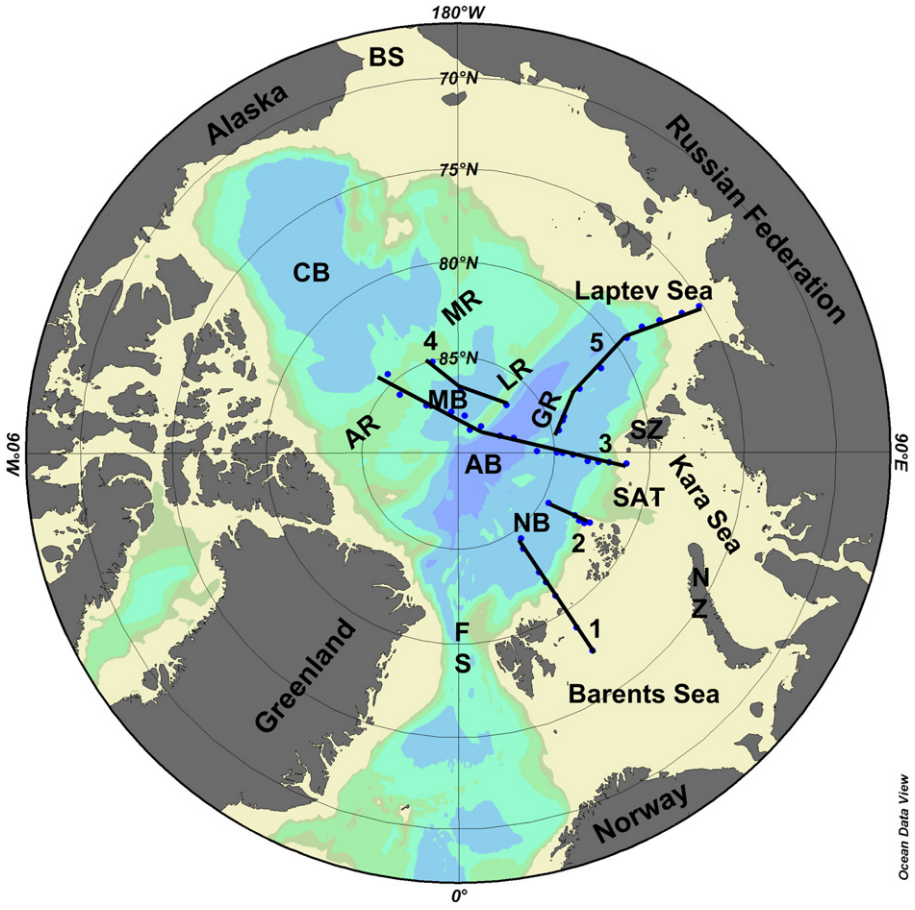

Fig. 1. Stations for trace metal sampling during ARK XXII/2. Transects are indicated by numbered lines as discussed in the same sequence in the text. Transect 1 goes from the Barents Sea into the Nansen Basin. Transect 2 also goes from the continental shelf into the Nansen Basin, just west of the St Anna Trough. Transect 3 goes from the continental shelf, east of the St Anna Trough, into the Nansen and Amundsen Basin, over the Lomonosov Ridge into the Makarov Basin and onto the Alpha Ridge. Transect 4 goes from the Mendeleyev Ridge into the Makarov Basin and extends until just in the Amundsen Basin. Transect 5 follows the deep Gakkel Ridge and extends into the Laptev Sea. AB: Amundsen Basin, AR: Alpha Ridge, BS: Bering Strait, CB: Canada Basin, FS: Fram Strait, GR: Gakkel Ridge, LR: Lomonosov Ridge, MB: Makarov Basin, MR: Mendeleyev Ridge, NB: Nansen Basin, NZ: Novaya Zemlya, SAT: St Anna Trough, SZ: Severnaya Zemlya.

Moreover, samples of the SAFe intercalibration program (Johnson et al., 2007) were analysed in triplicate (Table 1). It appears that the concentration of Al in bottle S #252 is slightly higher than the concentration for surface (S) water found by Brown and Bruland (2008), but not statistically different. Bottle S #425 is in almost perfect agreement, as is bottle D2 #3 for deep (D2) water from 1000 m.

2.5. Additional analyses

The salinity (conductivity), temperature and depth (pressure) were measured with two different CTDs of the same type (Seabird SBE 911+), one from the Netherlands Institute for Sea Research (NIOZ) and one from the Alfred Wegener Institute (AWI). Both had been calibrated before and after the expedition by the company (Seabird). Moreover, the conductivity sensors were calibrated during the expedition against salinity samples measured onboard (Schauer, 2008).

Inorganic nutrients (nitrate, nitrite, phosphate and silicate) were determined following procedures improved after Grasshoff et al. (1983). This colorimetric method measures the dissolved, monomeric orthosilicic acid ($Si(OH)_4$) and does not measure the polymeric, particulate or colloidal forms. Throughout this paper the mentioned silicate concentration is the same as the elemental concentration of Si in seawater.

Our laboratory has during the past 20 years taken part in intercomparison exercises organized by ICES and QUASIMEME. Most recently the 2006 exercise for Reference Material of Nutrients in Seawater was organized by the Meteorological Research Institute of Japan (Aoyama et al., 2008). Among 54 participating laboratories, the results of the better laboratories led to agreed average certified values and standard deviations, where our laboratory was the only one with all measured nutrients lying within a standard deviation of the agreed values. The samples were stored in a refrigerator and analysed usually within 10 h and always within 16 h on a Technicon TrAAcs 800 autoanalyser. The reproducibility of an internal laboratory standard mixture of silicate, phosphate and nitrate was measured daily and typically within 0.7% of its average value. For silicate specifically the reproducibility was 0.4% at an average value of 13.5 µM ($n=74$). Moreover, the deepest sample analysed of a station of 24 samples, was kept and reanalysed within the next run of the next station of 24 samples. The average absolute deviation between such duplicate analyses of the same sample yet measured twice in different runs was 0.131 µM for silicate at an average value of 8.17 µM ($n=23$). Due to this excellent agreement between two consecutive runs, no correction was needed for offsets between runs. Below we will compare values of dissolved (0.2 µm filtered) Al with unfiltered values of silicate, where by previous shipboard comparisons of filtered and unfiltered values of silicate (K. Bakker, unpublished work) we are confident there is no discernible difference within the analytical accuracy of the silicate values.

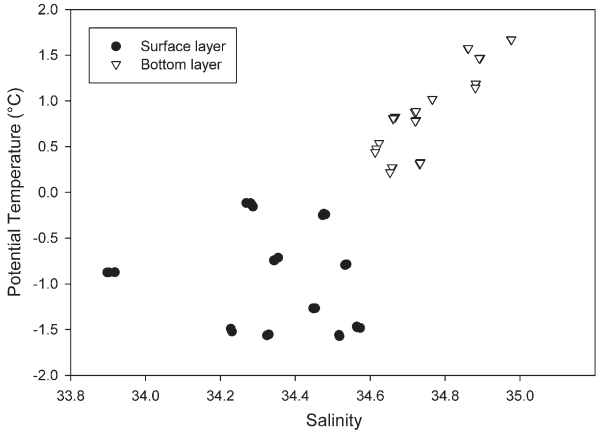

Fig. 2. Plot of potential temperature (°C) versus salinity for the Barents Sea in transects 1 and 2. Surface Layer Water (SLW) (closed circles) and Bottom Layer Water (BLW) with Atlantic influence (open triangles) were observed.

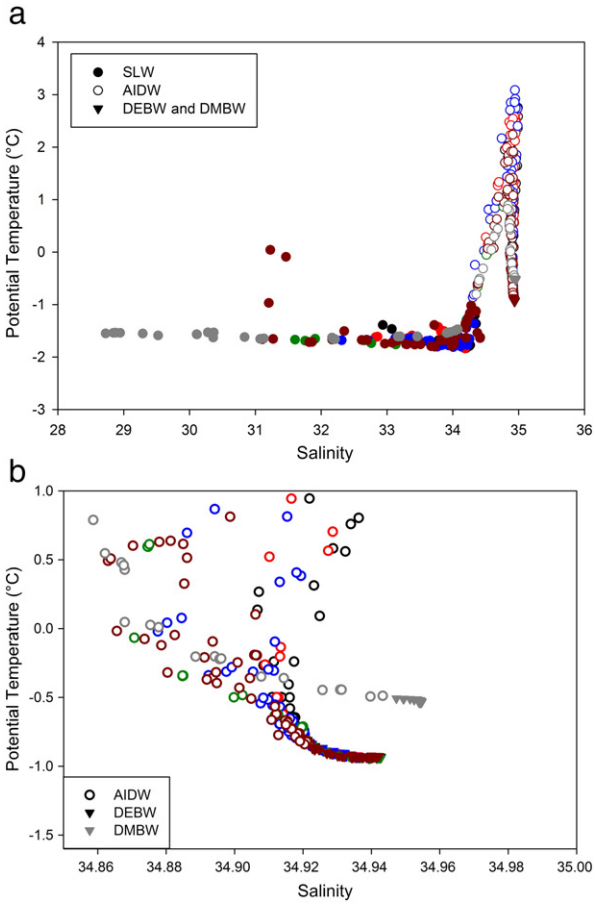

Fig. 3. Plots of potential temperature (°C) versus salinity for the Nansen, Amundsen and Makarov Basins of all transects. a) Upper graph: potential temperature (°C) versus salinity for the Nansen, Amundsen and Makarov Basins of all transects. Surface Layer Water (SLW) (closed circles), Atlantic and Intermediate Depth Water (AIDW) (open circles) and Deep Eurasian Basin Water (DEBW) and Deep Makarov Basin Water (DMBW) (closed triangles) were observed. Different colours are used for the different transects and basins; black for transect 1, red for transect 2, blue for the Nansen Basin transect 3, green for the Amundsen Basin transect 3 and 4, grey for the Makarov Basin transect 3 and 4 and brown for transect 5. b) Lower graph: potential temperature (°C) versus salinity for the deep Nansen, Amundsen and Makarov Basins of all transects at expanded scale. Atlantic and Intermediate Depth Water (AIDW) (open circles) and Deep Eurasian Basin Water (DEBW) and Deep Makarov Basin Water (DMBW) (closed triangles) are shown. Different colours are used for the different transects and basins; black for transect 1, red for transect 2, blue for the Nansen Basin transect 3, green for the Amundsen Basin transect 3 and 4, grey for the Makarov Basin transect 3 and 4 and brown for transect 5.

3. Hydrography

The Arctic Ocean comprises several basins separated by ridges (Fig. 1). The Canadian Basin comprises the deep Canada Basin (not studied) and the deep Makarov Basin. The latter Makarov Basin is separated by the fairly shallow Lomonosov Ridge (sill depth ranges from 1000 to 1600 m) from the Eurasian Basin. The Eurasian Basin is uniform down to about 4000 m depth, below which the deep Gakkel Ridge separates two sub-basins, the Nansen Basin and the Amundsen Basin.

The hydrographic features of the Eurasian and Makarov Basins have been described in detail by Anderson et al. (1994) and Rudels et al. (2000) and are briefly summarised here. Atlantic water flows

into the Eurasian Arctic basins via Fram Strait and the Barents Sea along the continental slope with the counterclockwise boundary current, influencing the surface and intermediate waters. The boundary current is modified by shelf processes and near the continent a branch crosses over the Lomonosov Ridge that separates the Eurasian Basin from the Makarov Basin while another branch flows along this ridge. The branch of the boundary current that crosses the Lomonosov Ridge influences the water column of the Makarov Basin. The formation of dense water on the shelves and subsequent slope convection influences the deepest parts of the water column in the Eurasian Basin.

Pacific water is flowing in through the Bering Strait over the Siberian shelves and mixes with the freshwater input of the Siberian rivers, creating strong stratification in the central Arctic Ocean. The Pacific inflow influences the water column of the Makarov Basin and this influence can extend into the surface layer of the Amundsen Basin. The Surface Mixed Layer (SML) is shallow, typically extending to 25 m depth in the central Arctic Ocean. Below the SML, there is an upper halocline in the Makarov Basin that sometimes extends into the Amundsen Basin. The upper halocline is marked by a nutrient maximum and is of Pacific origin. In the Nansen and Amundsen Basins the lower halocline is more profound, marked by a minimum in nitrate and nitrite.

Below the haloclines, the Atlantic Layer Water (ALW) is found, generally extending to about 600 m depth. The warmer and more saline ALW does not cross over the Lomonosov Ridge into the Makarov Basin due to a strong front in temperature and salinity over the Lomonosov Ridge. However, following the boundary current the Atlantic water flows into the Canadian Basin via the shelf edge. This results in a relatively colder less saline ALW in the Canadian Basin compared to the Eurasian Basin. Below about 800 m the Makarov Basin becomes warmer and more saline than water at a similar depth in the Eurasian Basin. This difference remains the case throughout the intermediate depth and deep basin waters. In the deep basins below the ALW, several water masses have been distinguished such as the Intermediate Depth Water (IDW) which is a mixture of overlying ALW and underlying Eurasian Basin Deep Water. Finally below the latter Eurasian Basin Deep Water one may find Eurasian Basin Bottom Water.

For the purpose of this paper the water column was divided in three major layers (Fig. 3) and occasionally minor sub-layers are also mentioned. The Surface Layer Water (SLW) is the cold and relatively fresh upper water layer. The SLW extended to depths of 75 to 150 m, and at its very surface includes the minor SML. The second layer, the Atlantic and Intermediate Depth Water (AIDW) generally extends until about 2000 m depth, and comprises the ALW with its characteristic potential temperature maximum and extending to about 600 m depth which is underlain by the Intermediate Depth Water over the 600 to 2000 m depth range. Within the Intermediate Depth Water the potential temperature decreased with increasing depth. Deeper than about 2000 m depth the potential temperature remained relatively constant while the salinity increased. To make the distinction between the AIDW and the underlying water layer, the Deep Eurasian Basin Water (DEBW), a cut off was made at a potential temperature of −0.8 °C. The DEBW comprises both Eurasian Basin Deep Water and Eurasian Basin Bottom Water. In the Makarov Basin the same water layers were distinguished, only the deepest layer was called Deep Makarov Basin Water (DMBW) and the cut off was made at a potential temperature of −0.4 °C because the deep water is warmer in the Makarov Basin (see above).

4. Results

4.1. Sampling along five transects

Samples were taken aboard Polarstern during expedition ARK XXII/2 from 28 July until 07 October 2007 from Tromsø (Norway) to Bremerhaven (Germany). The Arctic Basin was sampled in five transects numbered 1–5 in sequence of the actual cruise track. Along these 5 transects overall 44 stations (of which 27 were deeper than 2000 m) were sampled for dissolved Al. Transects three and four covered the Makarov Basin as well as the Eurasian Basin (Fig. 1). The 44 deployments of the all-titanium CTD sampling system with 24 GO-FLO samplers, resulted in a total of 666 samples that were analysed for Al because usually not all 24 GO-FLO samplers were sampled for Al. This is due to the seawater requirements of other cruise participants and the occasional malfunctioning of a GO-FLO sampler. Of the 666 samples analysed for Al, 10 samples (1.5%) were suspected outliers and therefore not further used in the data analyses and figures here presented. The complete data set including the 10 flagged outliers is available in the Pangaea database http://www.pangaea.de.

4.2. Transect 1

Transect 1 (Fig. 1) consisted of seven vertical profiles, of which three were over the continental shelf (Barents Sea) with a depth of

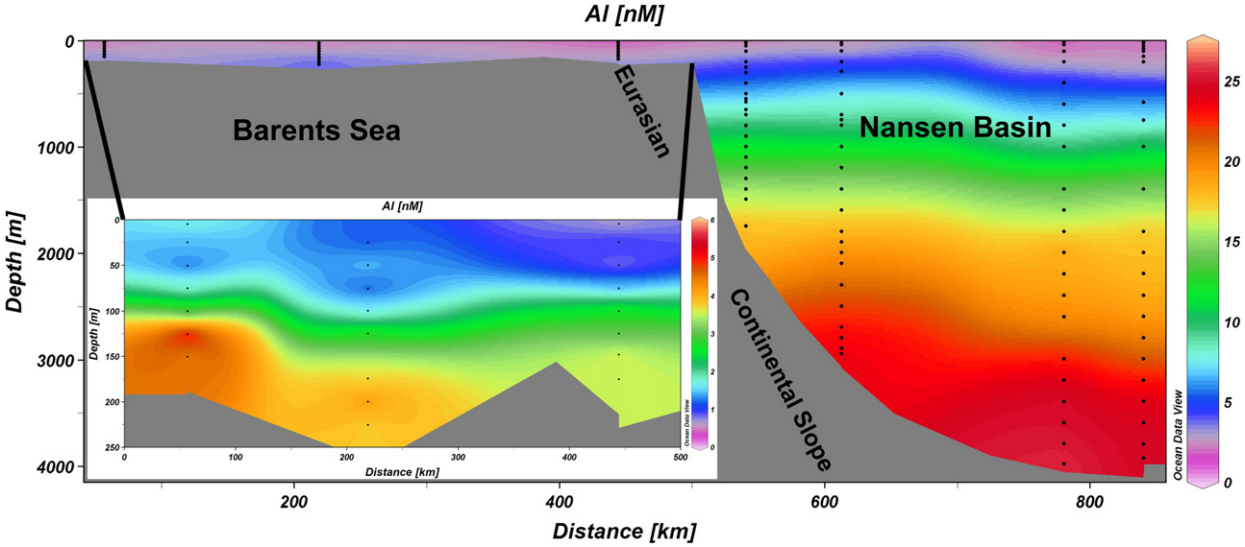

Fig. 4. Concentrations of dissolved aluminium (nM) over the entire water column in transect 1. The concentrations of Al in the Barents Sea are shown in the inset at the bottom left. Note the different colour scale for the Barents Sea. From this figure three suspected outliers were omitted.

approximately 200 m. Two profiles were sampled over the continental slope and two in the deep Nansen Basin (approximately 4000 m deep).

In the shallow Barents Sea the cold and relatively fresh SLW extended until about 75 m depth. The underlying Bottom Layer Water (BLW) had a higher salinity and potential temperature than the surface water (Fig. 2) indicating this was influenced by the Atlantic water flowing into the Arctic Ocean (see above 3. Hydrography).

In the Nansen Basin (slope and deep stations) the SLW extended to about 75 m depth close to the shelf and to over 100 m depth further into the deeper basin. Deeper than about 2000 m depth, in the DEBW, the potential temperature remained relatively constant whereas the salinity increased (Fig. 3b). Although the potential temperature was relatively constant in the DEBW it continued to decrease with depth until a slight potential temperature minimum around 3000 m depth.

The concentrations of dissolved Al for the entire water column are shown in Fig. 4. Over the continental shelf of the Barents Sea the concentrations of Al close to the surface were about 1 nM and increased to 3 nM at 100 m depth just below the SLW. Below 100 m the concentrations increased to almost 5 nM towards the sediments at around 200 m depth.

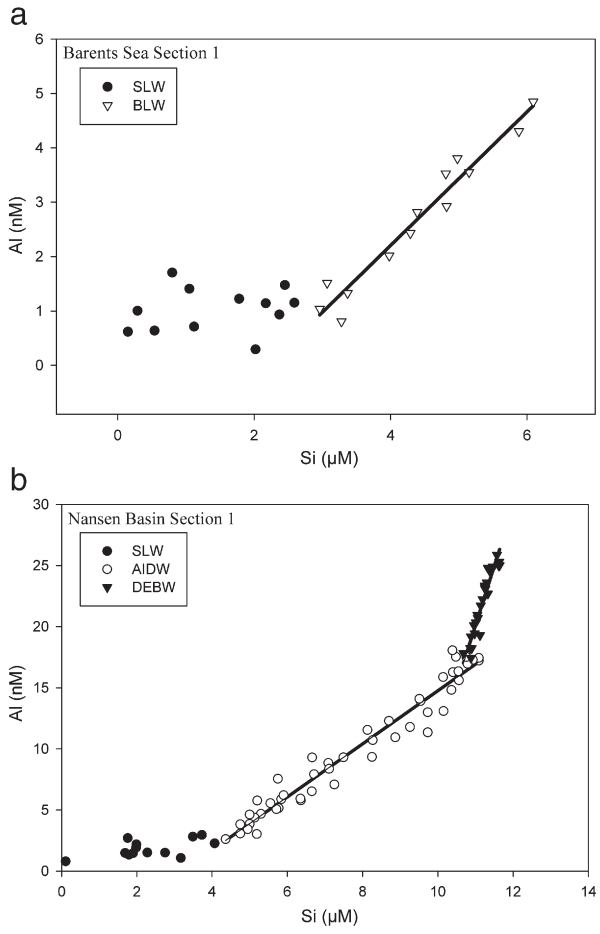

Fig. 5. Concentrations of dissolved Al (nM) versus dissolved Si (μM) in transect 1. a) Upper graph: concentrations of dissolved Al (nM) versus concentrations of dissolved Si (μM) over the continental shelf of transect 1 in the Surface Layer Water (SLW) (closed circles) and Bottom Layer Water (BLW) with Atlantic influence (triangles). Correlation in BLW [Al][nM] = 1.2[Si][μM] − 2.7 with $R^2 = 0.95$ $n = 13$ and $P < 0.001$ (Eq. (1)). b) Lower graph: concentrations of dissolved Al (nM) versus concentrations of dissolved Si (μM) in the Nansen Basin of transect 1 in the Surface Layer Water (SLW) (closed circles), Atlantic and Intermediate Depth Water (AIDW) (open circles) and Deep Eurasian Basin Water (DEBW) (closed triangles). Correlation in AIDW [Al][nM] = 2.2[Si][μM] − 7.0 with $R^2 = 0.96$ n = 48 and $P < 0.001$ (Eq. (2)). Correlation in DEBW [Al][nM] = 9.7[Si][μM] − 86.4 with $R^2 = 0.90$ n = 27 and $P < 0.001$ (Eq. (3)).

Over the continental slope the concentrations in the SML were slightly higher, approximately 1.5 nM, but also increased to 3 nM at 100 m depth. Further into the deeper basin the concentrations of Al in the SML were just below 1.5 nM and increased slightly to 2 nM just below the SLW. The concentration of Al increased steadily with depth to a maximum concentration of over 25 nM in the deep Nansen Basin. The highest concentrations of Al were not found at the greatest sampled depth but just below the potential temperature minimum. Looking from the basin towards the continental slope the concentrations of Al near the slope were elevated with respect to the same depths further into the basin. This effect was most profound at depths greater than 2000 m.

No correlation was found between the low concentrations of Al and Si in the SLW over the continental shelf (Barents Sea) of transect 1 (Fig. 5a). However, when looking at the relation in the BLW, a clear linear correlation was distinguished (Eq. (1); Table 2).

Similarly, in the SLW of the Nansen Basin no correlation was found between Al and Si (Fig. 5b). However, in the AIDW a clear correlation with a steeper slope than observed in the BLW over the shelf was found between Al and Si (Eq. (2); Table 3). To compare the slopes of the correlations observed, the Student's *T*-test for comparing two slopes as described by Zar (1999) was used. The slope of the Al-Si relation in the AIDW (Eq. (2)) was significantly steeper ($P = 0.001$, 2-tailed *T*-test) than in the BLW over the shelf (Eq. (1)).

From about 2000 m depth downwards in the DEBW the concentration of Al increased above 18 nM. Here the relation between Al and Si changed and the slope of the correlation became much steeper (Eq. (3); Table 4), indicative of a relative enrichment of Al with respect to Si in the deep basin. The slope of the Al–Si relation in the DEBW (Eq. (3)) was significantly steeper ($P < 0.001$, 2-tailed *T*-test) than in the AIDW (Eq. (2)).

4.3. Transect 2

Transect 2 (Fig. 1) consisted of five vertical profiles. Two profiles on the slope and two profiles on the shelf in the Barents Sea are shown in a colour plot (Fig. 6). The fifth profile in the deep Nansen Basin is only shown as a vertical profile (Fig. 7) to avoid excessive interpolation between this station and the other four stations further south. Above the continental shelf again cold, relatively fresh SLW (Fig. 2) was observed, but this extended only to a depth of 25 m. Below 25 m depth the BLW with Atlantic influence was warmer and more saline. The cold and relatively fresh SLW extended to only 25 m depth at the two stations over the continental slope but to 100 m depth at the station further into the deep basin. The potential temperature versus salinity distribution in the remainder of the water column was similar to what was found in transect 1 (see *subsection* 4.2.). In the DEBW a potential temperature minimum was observed at 3200 depth.

Over the shelf the concentrations of Al increased from around 1 nM in the SLW to 4 nM at 100 m depth (Fig. 6). At the shallowest station (250 m depth) the concentration of Al below the SLW remained relatively constant throughout the water column around 4 nM. At the deeper shelf station (300 m) closer to the basin the concentrations increased towards the sediment to 6 nM.

On the continental slope the concentrations of Al increased from around 1 nM in the SLW to 4 nM at 100 m depth, as observed on the shelf. Deeper, the concentrations of Al increased steadily to a

Table 2
Correlations between concentrations of dissolved Al (nM) and concentrations of dissolved Si (μM) in the bottom layer over the continental shelves (Barents Sea) of transect 1 and transect 2.

Shelf transect 1	Shelf transect 2
$[Al] = 1.2[Si] - 2.7$ $R^2 = 0.95$ $n = 13$ (1)	$[Al] = 3.3[Si] - 11.0$ $R^2 = 0.73$ $n = 11$ (4)

Note the difference of a factor 1000 between the concentration of Al in nM and the concentration of Si in μM.

Table 3
Correlations between concentrations of dissolved Al (nM) and concentrations of dissolved Si (μM) per basin and per transect for the Atlantic and Intermediate Depth Water (AIDW).

Basin	Nansen AIDW	Amundsen AIDW	Makarov AIDW
Transect 1	$[Al] = 2.2[Si]-7.0\ R^2 = 0.96 n = 48$ (2)	x	x
Transect 2	$[Al] = 2.2[Si]-6.1\ R^2 = 0.97 n = 37$ (5)	x	x
Transect 3	$[Al] = 2.2[Si]-7.8\ R^2 = 0.95 n = 45$ (7)	$[Al] = 2.2[Si]-8.9\ R^2 = 0.98 n = 15$ (9)	$[Al] = 2.0[Si]-9.7\ R^2 = 0.94 n = 24$ (11)
Transect 4	x	$[Al] = 2.2[Si]-8.4\ R^2 = 0.99 n = 9$ (14)	$[Al] = 1.9[Si]-9.1\ R^2 = 0.93 n = 12$ (12)
			$[Al] = 1.9[Si]-9.8\ R^2 = 0.94 n = 10$ (13)
Transect 5	$[Al] = 2.2[Si]-8.0\ R^2 = 0.93 n = 39$ (16)	$[Al] = 2.2[Si]-8.0\ R^2 = 0.93 n = 39$ (16)	x

Note the difference of a factor 1000 between the concentration of Al in nM and the concentration of Si in μM. The Eq. (16) for transect 5 was observed over the deep Gakkel Ridge and therefore presented in the columns of both the Nansen Basin and Amundsen Basin. The Eq. (12) was observed over the deeper Mendeleyev Ridge of transect 4 and therefore displayed separately. When combining all data of the AIDW in the Eurasian basin the following Eq. (18) was observed: $[Al] = 2.2[Si] - 7.7$; $R^2 = 0.94$; $n = 193$; $P < 0.001$.

Table 4
Correlations between concentrations of dissolved Al (nM) and concentrations of dissolved Si (μM) per basin and per transect for the and Deep Eurasian Basin Water (DEBW).

Basin	Nansen DEBW	Theoretical terrigenous component	Amundsen DEBW	Theoretical terrigenous component
Transect 1	$[Al] = 9.7[Si]-86.4\ R^2 = 0.90 n = 27$ (3)	2.27%	x	
Transect 2	$[Al] = 13.5[Si]-128.0\ R^2 = 0.91 n = 13$ (6)	3.41%	x	
Transect 3	$[Al] = 12.8[Si]-120.0\ R^2 = 0.83 n = 24$ (8)	3.18%	$[Al] = 10.3[Si]-92.7\ R^2 = 0.90 n = 17$ (10)	1.98%
Transect 4	x		$[Al] = 7.4[Si]-61.8\ R^2 = 0.94 n = 5$ (15)	1.56%
Transect 5	$[Al] = 9.8[Si]-88.0\ R^2 = 0.87 n = 43$ (17)	2.30%	$[Al] = 9.8[Si]-88.0\ R^2 = 0.87 n = 43$ (17)	2.30%

Note the difference of a factor 1000 between the concentration of Al in nM and the concentration of Si in μM. The Eq. (17) for transect 5 was observed over the deep Gakkel Ridge and therefore presented in the columns of both the Nansen Basin and Amundsen Basin. The theoretical terrigenous component in the DEBW is the result of solving Eq. (19) (see *subsection* 5.5.) for the specific transect and basin.

maximum of 24 nM Al at the deepest point of 3000 m depth. Further north in the deep Nansen Basin the concentration of Al in the SML of 1 nM (Fig. 7) was lower than the SML concentration found in the deep Nansen Basin at transect 1. However, at 100 m depth the concentration was 2 nM, just like in transect 1 (see *subsection* 4.2.). With increasing depth, the concentration of Al increased to over 26 nM with the highest concentrations just below the potential temperature minimum. Again as in transect 1, (see *subsection* 4.2.) the concentrations of Al were relatively higher towards the continental slope compared to the deep basin, especially at depths greater than 2000 m.

The relation between the concentrations of Al and Si in the BLW over the continental shelf was relatively modest (Eq. (4); Table 2).

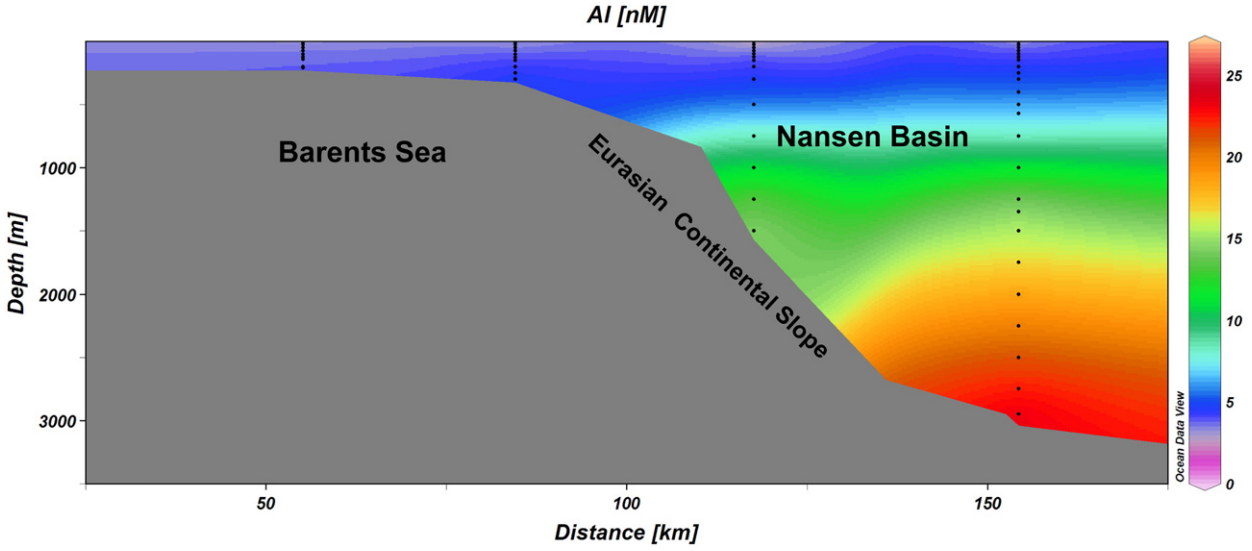

Fig. 6. Concentrations of dissolved Aluminium (nM) in the Barents Sea and over the continental slope in transect 2. From this figure one suspected outlier was omitted.

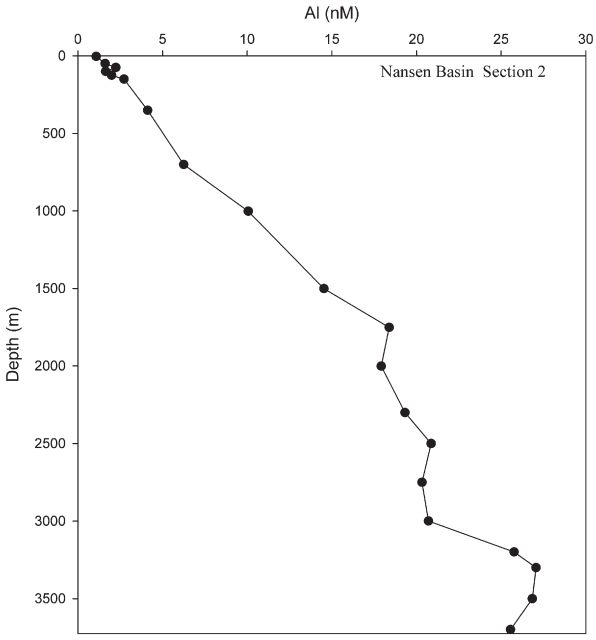

Fig. 7. Vertical profile of dissolved Al (nM) in the deep Nansen Basin of transect 2. From this figure one outlier (at 25 m depth) was omitted.

This modest correlation was probably caused by the relatively constant concentrations of Si above the shelf, ranging from 4.3 to 5.1 μM below the SLW, which was a much smaller variation in concentration than seen at transect 1 (2.4 to 6.1 μM, 3.2.).

In the basin, the relation between Al and Si was very similar to transect 1 (see *subsection* 4.2.), showing no apparent correlation in the SLW (Fig. 8). Yet below the SLW again a clear correlation was found in the AIDW of transect 2 (Eq. (5); Table 3) with almost the same slope as found in the AIDW in transect 1 (Eq. (2); Table 3). No significant difference between the slopes of these two Al–Si relationships (Eqs. (2) and (5)) was found ($P=0.86$, 2-tailed T-test). The slope of the relation became much steeper again in the DEBW where concentrations of Al increased above 18 nM (Eq. (6); Table 4). The slope of this Al–Si relation in the DEBW in transect 2 was steeper than the slope found in the DEBW in transect 1 (Eq. (3); Table 4) and the difference between these slopes (Eqs. (3) and (6)) was highly significant ($P<0.008$, 2-tailed T-Test).

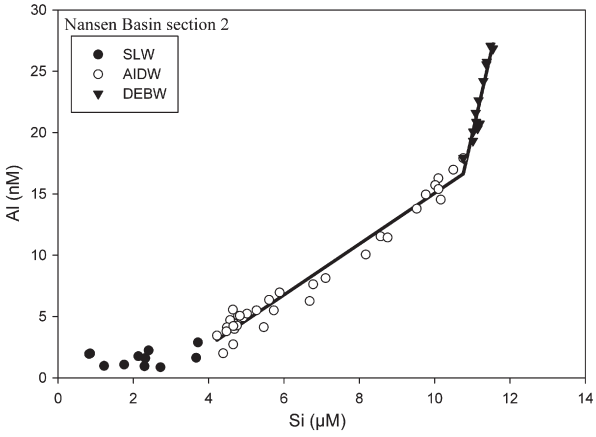

Fig. 8. Concentrations of dissolved Al (nM) versus concentrations of dissolved Si (μM) in the Nansen Basin of transect 2 in the surface layer water (SLW) (closed circles), Atlantic and Intermediate Depth Water (AIDW) (open circles) and Deep Eurasian Basin Water (DEBW) (closed triangles). Correlation in AIDW [Al][nM] = 2.2[Si][μM] − 6.1 with $R^2=0.97$ $n=37$ and $P<0.001$ (Eq. (5)). Correlation in DEBW [Al][nM] = 13.5[Si][μM] − 128.0 with $R^2=0.91$ $n=13$ and $P<0.001$ (Eq. (6)).

4.4. Transect 3

Transect 3 (Fig. 1) was by far the longest and had the most stations (17), crossing both the Eurasian and Makarov Basins and extending onto the Alpha Ridge. This transect is discussed in more detail to gain insight into the differences between the Nansen, Amundsen and Makarov Basins.

In the Nansen Basin the cold and relatively fresh SLW extended to about 50 m depth over the shelf and to 100 m depth in the basin. Below the SLW the ALW was warmer close to the Eurasian shelf and became progressively cooler further into the basins away from the Eurasian shelf (Fig. 9a and b). Below the ALW, in the IDW, the potential temperature decreased. In the DEBW there was a potential temperature minimum at 3000 m depth in the centre of the Nansen Basin, whereas in the deeper Amundsen Basin this minimum was located at approximately 3500 m depth. The SLW in the Amundsen Basin extended to a similar depth as in the Nansen Basin (100–125 m). In the Makarov Basin the SLW extended to 100 m depth close to the Lomonosov Ridge and to 150 m towards the Alpha Ridge. Furthermore, the Makarov SLW was relatively fresh compared to the SLW in the Eurasian Basin (Fig. 3a). The ALW in the Makarov Basin was colder compared to the Eurasian Basin while the intermediate and deep waters were warmer (Fig. 9a and b), which confirms what is known about the hydrography (see above 3. Hydrography). In the deep Makarov Basin there was no potential temperature minimum observed.

The SML concentrations of Al in transect 3 were generally below 1 nM with a slight elevation to 1.5 nM in the middle of the Amundsen Basin and the shelf of the Nansen Basin (Fig. 10a). The SML concentrations of Al were lowest (all concentrations <1 nM) in the Makarov Basin and onto the Alpha Ridge.

In the upper water column the concentrations of Al increased to over 4 nM at 250 m depth in the Nansen Basin close to the shelf and to 2 nM in the Amundsen Basin. In the Makarov Basin and towards the Alpha Ridge this increase in Al was absent and concentrations remained below 1.5 nM in the upper 300 m (Fig. 10a and b). The higher concentrations of Al coincided with the higher potential temperature of the ALW that flows in from the Eurasian side of the Eurasian Basin (Fig. 9a). In contrast, in the Makarov Basin there was a layer visible with lower concentrations of Al. These low concentrations of Al coincided with higher concentrations of Si (Fig. 11a and b). However, the core of the high concentrations of Si appears to be located deeper than the core of the low concentrations of Al. The reason that the cores of high Si and low Al are somewhat vertically resolved is most likely the biological uptake in the upper surface layer decreasing both the concentrations of Si and Al. The high concentrations of Si were associated with the upper halocline due to inflowing water of Pacific origin (Anderson et al., 1994). This shows the Pacific inflow delivers more Si, but not more Al to the surface waters of the Makarov Basin.

Below the SLW and the AIDW the concentrations of Al increased with depth to 26 nM in the Nansen Basin and to 24 nM in the Amundsen Basin (Fig. 10 b). At stations in the centre of the Nansen Basin, the maximum concentrations of Al were usually at or near the greatest depth in transect 3. This is in contrast to the other transects 1 and 2, where in the central Nansen Basin the maximum Al value is not near the bottom but some 400–600 m higher close to the observed potential temperature minimum. At stations towards the continental slope and close to the Gakkel Ridge in the Nansen Basin (i.e. not in the centre of the basin) in transect 3, the maximum concentrations of Al coincided again with the lowest potential temperature.

In the Amundsen Basin the maximum concentrations of Al are found at or just below the potential temperature minimum. In general, the concentrations of Al towards the continental slope appeared to be relatively higher compared to the concentrations at the same depths in the centre of the basin.

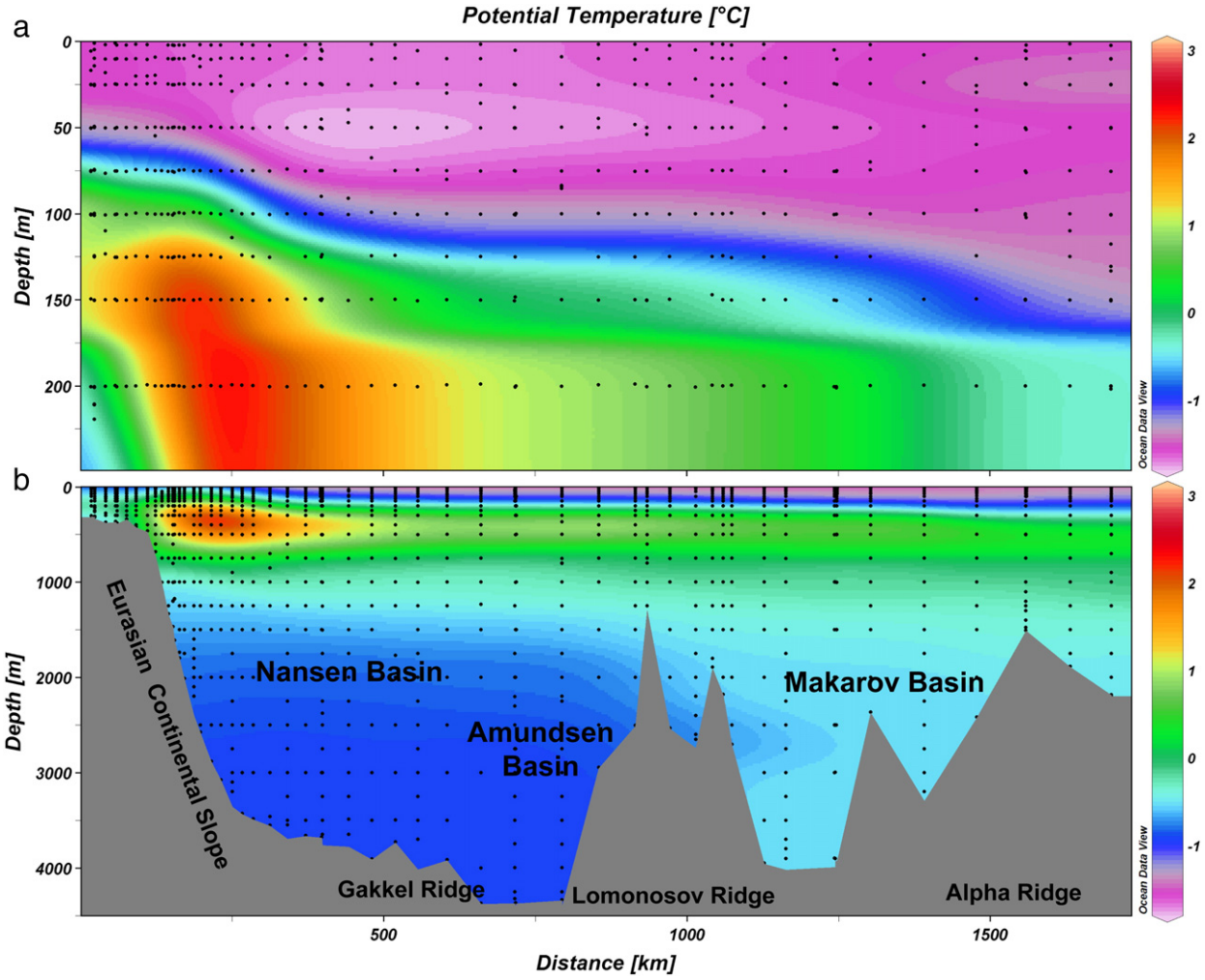

Fig. 9. a and b. Potential temperature (°C) in the upper 250 m of the water column (upper graph, a) and over the entire water column (lower graph, b) in transect 3. Potential temperature data from stations not sampled for trace metals are courtesy of the oceanography group of ARKXXII/2 (Schauer, 2008).

The concentrations of Al in the deep Makarov Basin (which does not show a potential temperature minimum) increased to a maximum of only 19 nM. This Al maximum was found at the greatest sampled depth.

When plotting the concentrations of Al versus the potential temperature between the three deep basins (deeper than 2000 m) of transect 3 (Fig. 12a and b) the above described clear distinctions are apparent.

For transect 3 the relationship between Al and Si in each basin is plotted for comparison between the basins. In the Nansen Basin (Fig. 13a) the low Al concentrations in the SLW showed no apparent correlation with Si. With increasing depth, in the AIDW, the increasing concentrations of Al showed a clear linear correlation with the concentrations of Si (Eq. (7); Table 3). The slope of this relation in the AIDW in the Nansen Basin in transect 3 is very close to the slopes observed for the AIDW in the Nansen Basin in transects 1 and 2 (Eqs. (2) and (5); Table 3). Indeed there were no significant differences when comparing the slopes (Eqs. (2), (5) and (7)) of the Al–Si relations in the AIDW in the Nansen Basin between the transects 1, 2 and 3 ($P > 0.48$ in all cases, 2-tailed T-test).

The concentration of Al increased with increasing depth to concentrations above 18 nM, at approximately 2000 m in the deep Nansen Basin. Below 2000 m depth, in the DEBW, the slope of correlation was steeper once again (Eq. (8); Table 4). The Al–Si relation in the DEBW in this part of the Nansen Basin in transect 3 seems to be similar to the one observed in the DEBW in transect 2 (Eq. (6); Table 4). Indeed, no significant difference was found between the slopes (Eqs. (6) and (8)) of these Al–Si relations ($P = 0.76$, 2-tailed T-test). There was, however, a significant difference between the slopes of the Al–Si relations in the DEBW from transect 1 (Eq. (3); Table 4) and the DEBW in the Nansen Basin in transect 3 (Eq. (8)) ($P = 0.024$, 2-tailed T-Test).

There were far fewer data points in the Amundsen Basin but these data show an almost identical pattern with a similar enrichment of Al with respect to Si in the DEBW (Fig. 13b) as seen for the Nansen Basin (Fig. 13 a). The slope of the Al–Si relation in the AIDW of the Amundsen Basin (Eq. (9); Table 3) was almost identical to the regression slope of the AIDW in the Nansen Basin (Eq. (7); Table 3) in this same transect 3. Indeed the difference between the slopes (Eqs. (7) and (9)) of the Al–Si relations in the AIDW in the Nansen versus the Amundsen Basin in transect 3 was insignificant ($P = 0.95$, 2-tailed T-test). Moreover, there was also no significant difference between the slopes of the Al–Si relation in AIDW of the Nansen Basin observed in transects 1 and 2 (Eqs. (2) and (5); Table 3) and the slope observed in the AIDW in the Amundsen Basin (Eq. (9)) in transect 3 ($P = 0.80$ and $P = 0.69$, respectively, 2-tailed T-test).

The slope of the Al–Si relation in the DEBW in the deep Amundsen Basin in transect 3 was once again much steeper (Eq. (10); Table 4). However, this slope was not as steep as in the DEBW in the Nansen Basin in transect 3 (Eq. (8); Table 4). The differences in slope of the

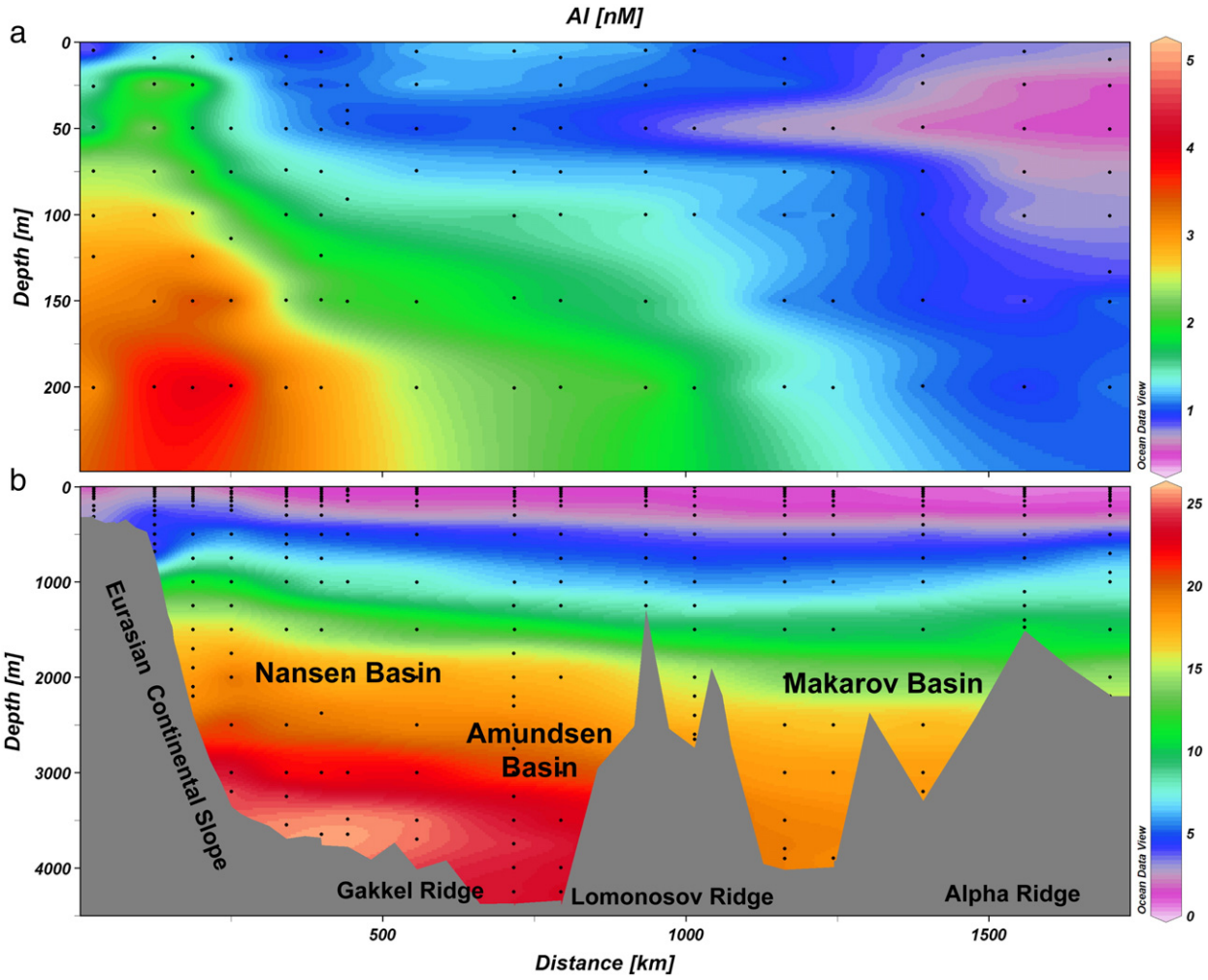

Fig. 10. a and b. Concentrations of dissolved aluminium (nM) in the upper 250 m of the water column (upper graph, a) and over the entire water column (lower graph, b) in transect 3. Note the different colour scale in the upper 250 m of the water column (upper graph, a). Five (5) suspected outliers were omitted from these figures.

Al–Si relation between the DEBW in the Amundsen Basin (Eq. (10)) in transect 3 was significant when compared to the DEBW in the Nansen Basin in transect 2 (Eq. (6); $P=0.049$), but not significant compared to the DEBW in the Nansen Basin in transects 1 and 3 (Eq. (3) and (8); $P=0.58$ and $P=0.15$, respectively, 2-tailed T-test).

On the other side of the Lomonosov Ridge in the Makarov Basin and onto the Alpha Ridge there was again no apparent correlation in the SLW between the low concentrations of Al and the concentrations of Si, but the latter were much higher with concentrations up to 35 μM (Fig. 13c). In the underlying AIDW of the Makarov Basin, the slope of the relation between Al and Si (Eq. (11); Table 3) was less steep than in AIDW in the basins on the other side of the Lomonosov Ridge. The slope of the Al–Si relation in the AIDW of the Makarov Basin in transect 3 differed significantly from the slopes of the Al–Si relations (Eqs. (2), (5), (7) and (9); Table 3) found in the AIDW in the Nansen and Amundsen Basins in all transects ($P<0.05$ in all cases, 2-tailed T-test). Moreover, in the Makarov Basin the concentrations of Al continuously increased with depth within and below the AIDW, but this increase was less steep than in the Eurasian Basin as the concentrations of Al did not increase over a maximum 19 nM value in the deep layers of the Deep Makarov Basin Water (DMBW). The concentrations of Si on the other hand, decreased below a maximum value at 2500 m depth. Nevertheless, the deep Si values below 2500 m depth in the DMBW of the Makarov Basin still were relatively higher compared to the deep Si values in the DEBW of the Eurasian Basin (Fig. 11b). Overall, the less steep slope of the Al–Si relation in the AIDW, the Si maximum at 2500 m depth and the relatively high concentrations of Si in the DMBW all are indicative of a relative enrichment of Si, most likely of Pacific origin, in the Makarov Basin.

4.5. Transect 4

Transect 4 (Fig. 1) consisted of merely three vertical profiles for Al, one on the Mendeleyev Ridge, one in the Makarov Basin and one just in the Amundsen Basin close to the Lomonosov Ridge. These three profiles are shown as vertical profiles and not as colour plots to avoid excessive interpolation (Fig. 14). The distributions of potential temperature and salinity at the different stations were very similar to the observations in transect 3 (see *subsection* 4.4.).The cold, fresh SLW extended to greatest depth over the Mendeleyev Ridge (125 m), at intermediate depths in the Makarov Basin (between 125 and 100 m) and was shallowest in the Amundsen Basin (100 m). The SLW was relatively fresh on the Mendeleyev Ridge and became increasingly saline towards the Amundsen Basin whereas the ALW underneath became warmer as noted in transect 3 (see *subsection* 4.4.). Below the potential temperature maximum of the ALW the potential temperature and salinity were quite similar at all three stations until about 750 m depth. At greater depths exceeding 750 m, the water became colder and less saline in the Amundsen Basin relative to the water on the other side of the Lomonosov Ridge as was observed in transect 3 (see *subsection* 4.4.). In the DEBW in the Amundsen Basin there was a slight potential temperature minimum between 3500 and 3750 m depth.

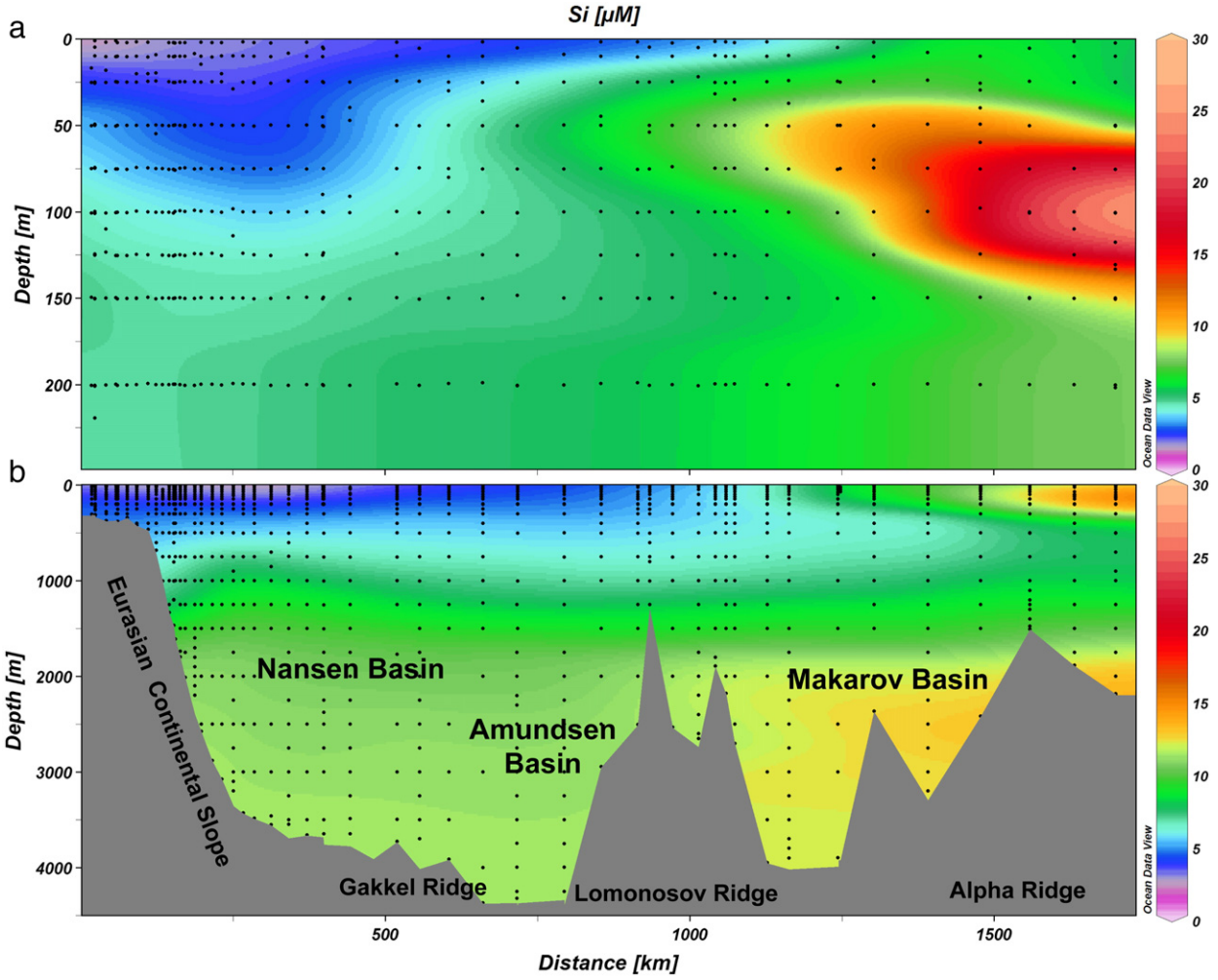

Fig. 11. a & b. Concentrations of dissolved silicate (µM) in the upper 250 m of the water column (upper graph, a) and over the entire water column (lower graph, b) in transect 3. Note the different colour scale in the upper 250 m of the water column (upper graph, a).

Above the Mendeleyev Ridge and in the Makarov Basin the concentrations of Al in the SLW were similar to those seen in transect 3 (see *subsection* 4.4.) above the Alpha Ridge and in the Makarov Basin, with concentrations staying below 1 nM in the SLW and reaching 1.5 nM around 250 m. In the Amundsen Basin the concentration of Al in the upper SLW was also below 1 nM but the concentration increased more rapidly reaching 2 nM around 250 m depth.

With increasing depth, the concentrations of Al increased to almost 19 nM near the bottom in the Makarov Basin and reached 23 nM at the potential temperature minimum in the Amundsen Basin. Over the Mendeleyev Ridge the concentration of Al was highest at about 15.5 nM at 1950 m, in proximity to the sediment (Fig. 14).

The slope of the relationship between Al and Si (Fig. 15a) on the Mendeleyev Ridge in the AIDW below the SLW (Eq. (12); Table 3) was slightly less steep than seen in the AIDW of the Makarov Basin in transect 3 (Eq. (11); Table 3). However, there was no significant difference between the slopes (Eqs. (11) and (12)) ($P=0.56$, 2-tailed *T*-test). The concentrations of Si in the surface waters in transect 4 were not as extreme as seen in transect 3 (see *subsection* 4.4.), but still quite high with a maximum of almost 18 µM.

In the AIDW in the Makarov Basin in transect 4 the Al–Si relationship (Eq. (13); Table 3), as shown in Fig. 15b, was similar to the one seen in the Makarov Basin in transect 3 (Eq. (11); Table 3) and no significant difference was found between the slopes ($P=0.64$, 2-tailed *T*-test) of Eqs. (11) and (13). Again the concentration of Si decreased deeper than 2500 m, as observed in the Makarov Basin in transect 3 (see *subsection* 4.4.).

The Al–Si relation in the AIDW of the Amundsen Basin in transect 4 (Eq. (14); Table 3), as shown in Fig. 15c, and was very similar to the one encountered in the AIDW in the Amundsen Basin in transect 3 (Eq. (9); Table 3). Indeed there was no significant difference between the slope of the Al–Si relation in the AIDW of the Amundsen Basin in transect 3 (Eq. (9)) compared to the slope in the AIDW in transect 4 (Eq. (14)) ($P=0.83$, 2-tailed *T*-test).

In the DEBW in the Amundsen Basin of transect 4, the regression slope (Eq. (15); Table 4) was less steep than the slope found in transect 3 for the DEBW in the Amundsen Basin (Eq. (10); Table 4), but the difference of slopes (Eqs. (10) and (15)) was insignificant ($P=0.30$, 2-tailed *T*-test). Finally the concentrations of Si in the DEBW of the Amundsen Basin were lower than those found at similar depths in the Makarov Basin, as was also observed in transect *3* (see *subsection* 4.4.).

4.6. Transect 5

The final transect sampled was over the Gakkel Ridge onto the continental slope and into the Laptev Sea (Fig. 1). The Gakkel Ridge is quite deep with depths between 4000 and 5200 m. The depth of 5200 m was observed in a deep trench just before the onset of the continental slope. The distributions of potential temperature and salinity (Fig. 3a and b) in the deep part were similar to previous

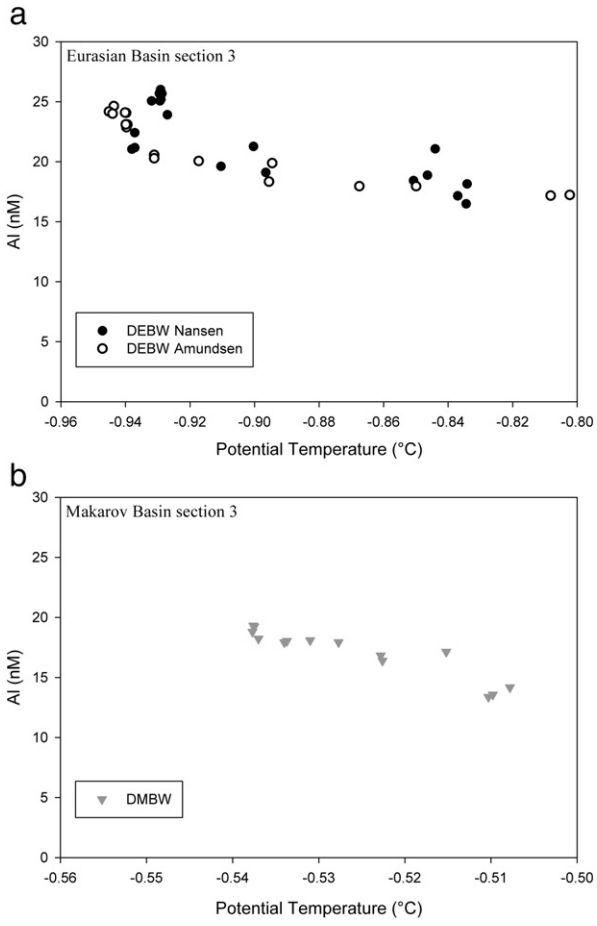

Fig. 12. Concentrations of dissolved aluminium (nM) versus potential temperature (°C). Note the difference in the Potential temperatures and concentrations of Al between the DEBW and DMBW. a) Upper graph: concentrations of dissolved aluminium (nM) versus potential temperature (°C) plot in the Deep Eurasian Basin Water (DEBW) of the Nansen Basin (closed circles) and Amundsen Basin (open circles). b) Lower graph: concentrations of dissolved aluminium (nM) versus potential temperature (°C) plot in the Deep Makarov Basin Water (DMBW).

observations in the Nansen and Amundsen Basins (see *subsections* 4.2, 4.3 and 4.4.). However, over the continental slope and onto the shelf there were some deviations. The cold and relatively fresh SLW extended to around 100 m depth in the deep parts of the basin and over the continental slope. At the onset of the continental slope the top of the SLW showed an increase in potential temperature compared to the top of the SLW further away from the continental slope (Fig. 16a). At the edge of the continental shelf, however, the potential temperatures were lower again and quite close to those observed over the deep parts of the Gakkel Ridge. This indicates a flow of a different, warmer water mass in the top of the SLW close to the continental shelf. The origin of this apparently distinct water mass is suspected to be warmer water brought up from below due to enhanced mixing (pers. com. Dr B. Rudels). Over the shelf (Laptev Sea) the water became warmer and less saline, with the upper parts of this shallow water column (55–35 m) being the warmest and least saline. The ALW was warmest over the continental slope and was colder further away from the slope (Fig. 16b) as was seen in transect 3 (see *subsection* 4.4.). In the part over the continental slope with bottom depths between 2000 and 1000 m the potential temperature values in this depth range were somewhat elevated compared to values at similar depths further away from the slope (Fig. 16b). In the DEBW of transect 5 there was a potential temperature minimum around 3000 m observed in all six stations deeper than 3000 m, which

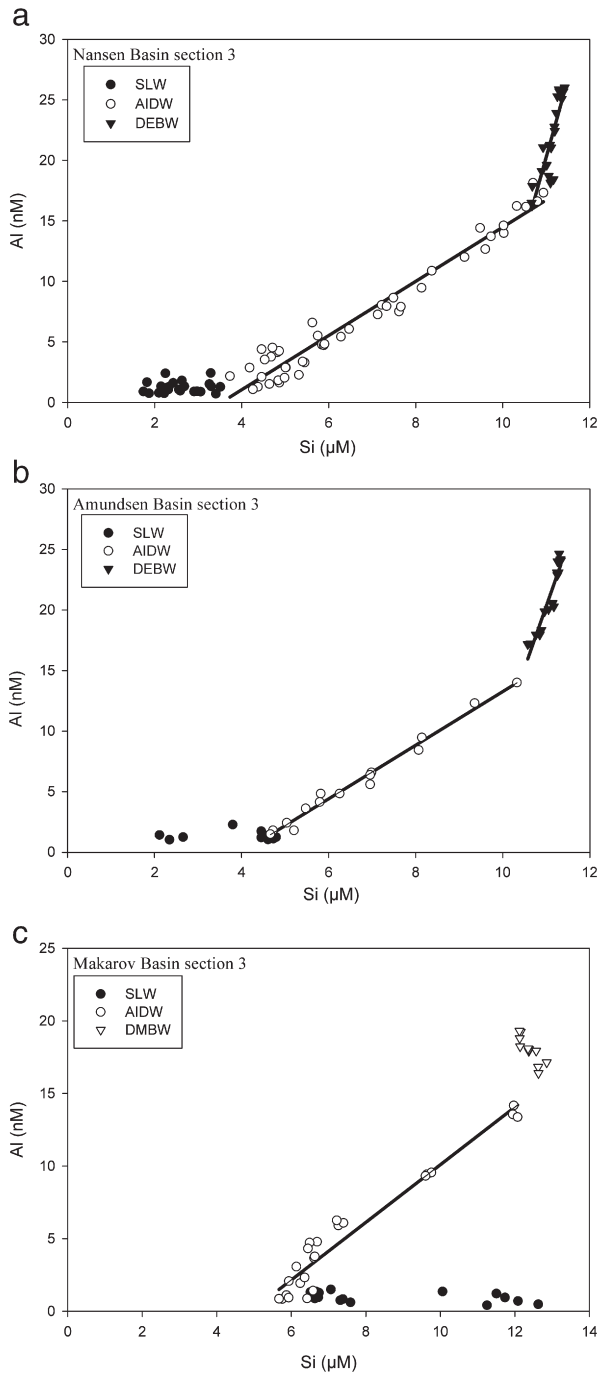

Fig. 13. Concentrations of dissolved Aluminium (nM) versus concentrations of dissolved Si (μM) in transect 3. a) Upper graph: concentrations of dissolved aluminium (nM) versus concentrations of dissolved Si (μM) in the Nansen Basin in transect 3 in the Surface Layer Water (SLW) (closed circles), Atlantic and Intermediate Depth Water (AIDW) (open circles) and Deep Eurasian Basin Water (DEBW) (closed triangles). Correlation in Nansen Basin AIDW [Al][nM] = 2.2[Si][μM] − 7.8 with $R^2 = 0.95$ $n = 45$ and $P < 0.001$ (Eq. (7)). Correlation in Nansen Basin DEBW [Al][nM] = 12.8[Si][μM] − 120.0 with $R^2 = 0.83$ $n = 24$ and $P < 0.001$ (Eq. (8)). b) Middle graph: concentrations of dissolved aluminium (nM) versus concentrations of dissolved Si (μM) in the Amundsen Basin in transect 3 in the Surface Layer Water (SLW) (closed circles), Atlantic and Intermediate Depth Water (AIDW) (open circles) and Deep Eurasian Basin Water (DEBW) (closed triangles). Correlation in Amundsen Basin AIDW [Al][nM] = 2.2[Si][μM] − 8.9 with $R^2 = 0.98$ $n = 15$ and $P < 0.001$ (Eq. (9)). Correlation in Amundsen Basin DEBW [Al][nM] = 10.3[Si][μM] − 92.7 with $R^2 = 0.90$ $n = 17$ and $P < 0.001$ (Eq. (10)). c) Lower graph: concentrations of dissolved aluminium (nM) versus concentrations of dissolved Si (μM) in the Makarov Basin in transect 3 in the Surface Layer Water (SLW) (closed circles), Atlantic and Intermediate Depth Water (AIDW) (open circles) and Deep Makarov Basin Water (DMBW) (open triangles). Correlation in Makarov Basin AIDW [Al[nM]] = 2.0[Si][μM] − 9.7 with $R^2 = 0.94$ $n = 24$ and $P < 0.001$ (Eq. (11)).

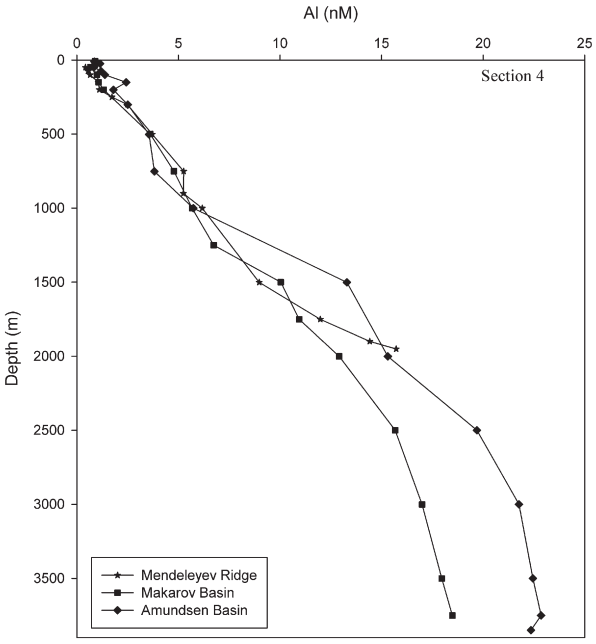

Fig. 14. Profiles of dissolved Al (nM) over the Mendeleyev Ridge, in the Makarov Basin and in the Amundsen Basin of transect 4.

were sampled for trace metals. At the two stations over the continental slope no potential temperature minimum was observed.

The concentrations of Al of transect 5 in the upper 250 m are shown in Fig. 17a. Furthest away from the continental shelf, over the deep parts of the Gakkel Ridge, the concentrations of Al in the SML were below 1 nM and values increased to 2 nM at approximately 200 m depth. Over the continental slope the Al distribution in the SLW became increasingly patchy with concentrations around 1 nM. The 2 nM Al isocline over the slope was located shallower than in the basin and rose to above 100 m towards the shelf edge, consistent with the suspected upwelling of deeper and warmer water with higher concentrations of Al. Deeper than these depths of the 2 nM Al isocline, the concentration of Al increased to over 3 nM in the warmer ALW. Low concentrations of Al below 1 nM were observed over the entire shallow (67 m) water column close to the edge of the continental shelf. The concentrations of Al increased to around 2 nM further onto the shelf. The low concentrations of Al coincided with lower potential temperature (Fig. 16a), indicating the suspected upwelling did not extend onto the shelf.

When looking at the total water column (Fig. 17b), the concentrations of Al showed a steady increase with depth. In the region furthest away from the slope the maximum concentrations encountered were approximately 24.5 nM at about 3500 m in the DEBW. The maximum Al values close to and in the deep trench, were just over 26.5 nM and 28 nM, respectively, and were also found around 3500 m. This depth of 3500 m was somewhat below the potential temperature minimum, but well above the sediments located around 4250 m depth.

Over the slope, the concentrations of Al deeper than 2000 m were relatively high compared to the same depths away from the slope. On the other hand, at the station over the slope shallower than 2000 m, the concentrations of Al around 1000 m appeared to be somewhat lower compared to the same depths further away from the slope. This coincided with the aforementioned (see above) elevated potential temperatures observed in the same region (Fig. 16b). These higher potential temperatures are suspected to be from dense water from the shelf that has entrained Atlantic water which is too warm to sink any further (pers. com. Dr B. Rudels). Unfortunately this water with elevated potential temperatures was not sampled further for Al than

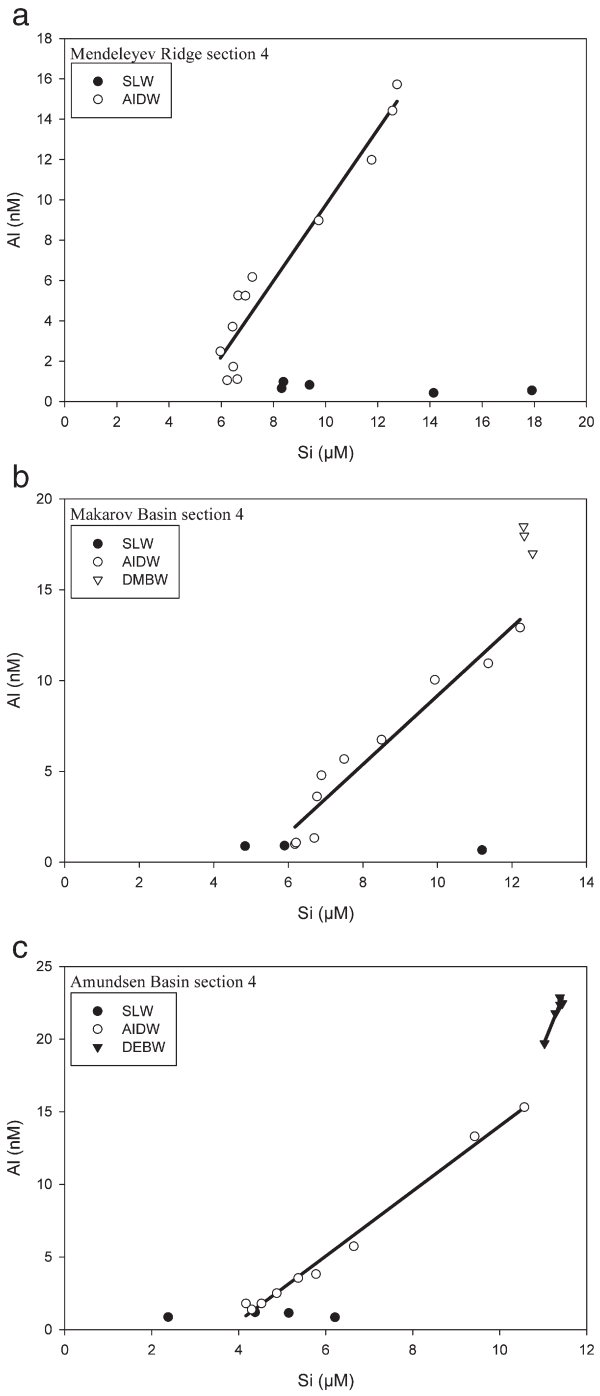

Fig. 15. Concentrations of dissolved aluminium (nM) versus concentrations of dissolved Si (μM) in transect 4. a) Upper graph: concentrations of dissolved aluminium (nM) versus concentrations of dissolved Si (μM) over the Mendeleyev Ridge in transect 4 in the Surface Layer Water (SLW) (closed circles) and Atlantic and Intermediate Depth Water (AIDW) (open circles). Correlation in Mendeleyev Ridge AIDW [Al][nM] = 1.9[Si][μM] − 9.1 with $R^2 = 0.93$ $n = 12$ and $P < 0.001$ (Eq. (12)). b) Middle graph: concentrations of dissolved aluminium (nM) versus concentrations of dissolved Si (μM) in the Makarov Basin in transect 4 in the Surface Layer Water (SLW) (closed circles), Atlantic and Intermediate Depth Water (AIDW) (open circles) and Deep Makarov Basin Water (DMBW) (open triangles). Correlation in Makarov Basin AIDW [Al][nM] = 1.9[Si][μM] − 9.8 with $R^2 = 0.94$ $n = 10$ and $P < 0.001$ (Eq. (13)). c) Lower graph: concentrations of dissolved aluminium (nM) versus concentrations of dissolved Si (μM) in the Amundsen Basin in transect 4 in the Surface Layer Water (SLW) (closed circles), Atlantic and Intermediate Depth Water (AIDW) (open circles) and Deep Eurasian Basin Water (DEBW) (closed triangles). Correlation in Amundsen Basin AIDW [Al][nM] = 2.2[Si][μM] − 8.4 with $R^2 = 0.99$ $n = 9$ and $P < 0.001$ (Eq. (14)). Correlation in Amundsen Basin DEBW [Al][nM] = 7.4[Si][μM] − 61.8 with $R^2 = 0.94$ $n = 5$ and $P = 0.006$ (Eq. (15)).

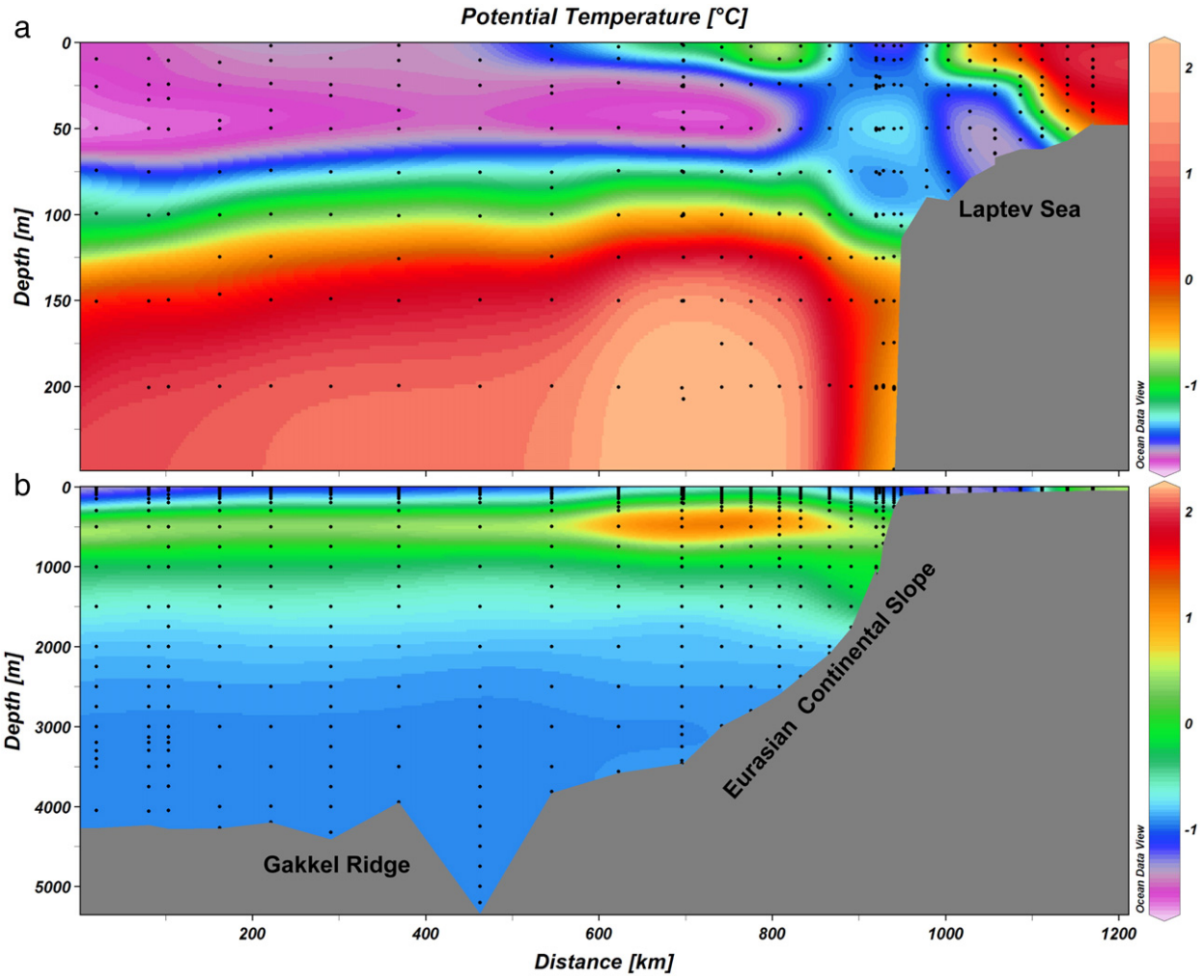

Fig. 16. a & b Potential temperature (°C) in the upper 250 m of the water column (upper graph, a) and over the entire water column (lower graph, b) in transect 5. Note the different colour scale in the upper 250 m of the water column (upper graph, a). Potential temperature data from stations not sampled for trace metals are courtesy of the oceanography group of ARKXXII/2 (Schauer, 2008).

the mentioned samples around 1000 m that are just at the top of this water. The lower concentrations of Al at this station would be related to the Atlantic water that has lower concentrations of Al than water generally observed at 1000 m depth.

The relationship between Al and Si for transect 5 (without the two shelf stations, Fig. 18)) in the AIDW over the Gakkel Ridge (Eq. (16); Table 3) was similar to the relations previously found in the AIDW of the Nansen Basin (Eqs. (2), (5) and (7); Table 3) and Amundsen Basin (Eqs. (9) and (14); Table 3) basins. Furthermore, no significant difference was found when comparing the slope (Eq. (16) of the Al–Si relation in the AIDW in transect 5 with the slopes (Eqs. (2), (5), (7), (9) and (14); Table 3) of the AIDW in the entire Nansen or Amundsen Basin ($P > 0.58$ in all cases, 2-tailed T-test).

In the DEBW over the Gakkel Ridge of transect 5 the slope of the relation (Fig. 18) became steeper once again (Eq. (17); Table 4). This slope was not as steep as seen previously for the DEBW in the Nansen Basin in transects 2 and 3(Eqs. (6) and (8); Table 4), but more similar to the slope seen in the deep Nansen Basin in transect 1 (Eq. (3); Table 4). Indeed, no significant difference was found when comparing the slope of the Al-Si relation in the DEBW of transect 5 (Eq. (17)) with the slope in the DEBW in transect 1 (Eq. (3); $P = 0.93$, 2-tailed T-test) and a significant difference when comparing with the slope of the Al-Si relation in the DEBW of transects 2 and 3 (Eqs. (6) and (8); $P < 0.05$ in both cases, 2-tailed T-test). No significant difference was found between the slope of the Al–Si relation (Eq. (17)) in the DEBW in transect 5 and those of the DEBW in the Amundsen Basin in the previous transects 3 and 4 (Eqs. (10) and (15); Table 4) ($P = 0.72$ and $P = 0.57$, respectively, 2-tailed T-test).

5. Discussion

5.1. Historic data

To the best of our knowledge there are no data available on dissolved aluminium in the central Arctic Ocean. However, there are data published by Moore (1981) and Measures (1999), but these are for reactive aluminium from unfiltered, non-acidified seawater samples.

In the deep waters Moore (1981) collected unfiltered seawater in GO-FLO samplers proven suitable for sampling trace metals (Bruland et al., 1979; De Baar et al., 2008) and found concentrations of reactive Al increasing from 18.2 nM at 1900 m to 21 nM at 2600 m depth in the Makarov Basin near the Lomonosov Ridge. Previously it has been assumed that more than 90% of the Al present in the water column resides in the dissolved phase (Measures, 1999). When for the sake of the argument using this previous assumption, then the dissolved concentrations should have been about 10% lower thus 16.4 and 18.9 nM, respectively. The latter range is in good agreement with the concentrations of dissolved Al reported here at the Lomonosov Ridge of 15 nM at 2000 m increasing to 18.1 nM at 2650 m found (see above *subsection* 4.4.).

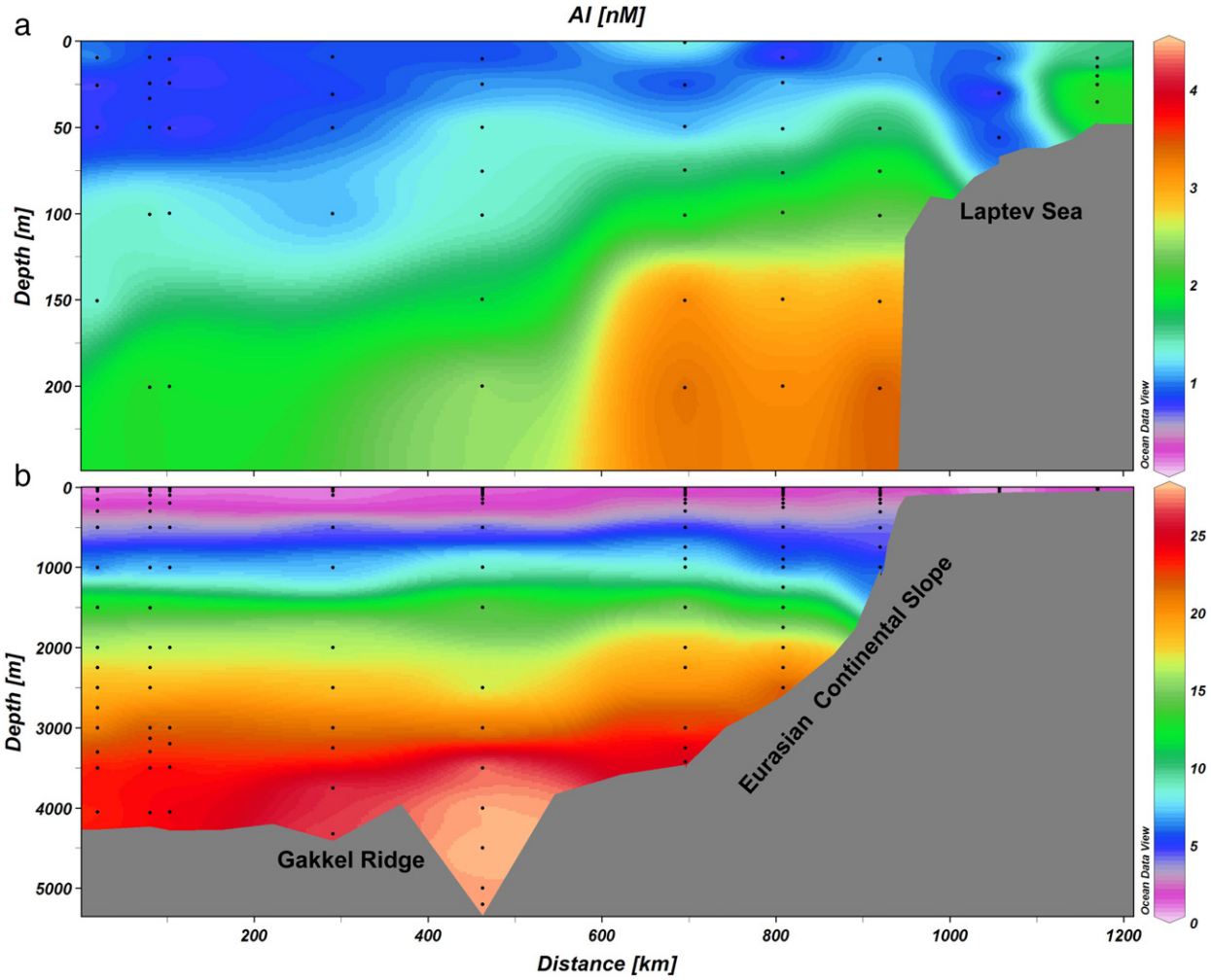

Fig. 17. a & b Concentrations of dissolved aluminium (nM) in the upper 250 m of the water column (upper graph, a) and over the entire water column (lower graph, b) in transect 5. Note the different colour scale in the upper 250 m of the water column (upper graph, a). From these figures one suspected outlier was omitted.

The concentrations of reactive Al found in the surface waters in the High Arctic near the Lomonosov Ridge by Moore (1981) are between 3 and 4.1 nM in the upper 130 m and also collected in GO-FLO samplers. Similarly, Measures (1999) found concentrations between 3 and 5.9 nM of reactive Al in surface waters in the same region in unfiltered seawater (see text below). These values are considerably higher than the surface concentrations of dissolved Al collected with GO-FLO samplers around the Lomonosov Ridge presented in this paper. These filtered surface water values of dissolved Al range between 0.6 and 1.3 nM in the upper 25 m and between 0.8 and 1.7 nM dissolved Al at 150 m depth on the Makarov and Amundsen Basin side, respectively, of the Lomonosov Ridge (see *subsection* 4.4.). Higher concentrations of reactive Al in surface waters of up to 22.4 nM in the Canadian Basin and up to 6.9 nM in the Eurasian Basin were observed by Measures (1999). Some 13 Al values (range 1.4 to 22.4 nM, average 8.4 nM S.D. = 6.8) were by collection in the very top 10–20 cm layer (including the sea-surface microlayer) by hand sampling (with double plastic gloves) into a pre-cleaned plastic bottle from the edge of an ice-floe positioned upwind of the ship. Moreover, some 39 samples had been collected with modified Niskin type PVC sampling bottles for shallow depths down to 28 m, yielding values of Al ranging from 2.4 to 22.2 nM with an average of 6.9 nM (S.D. = 4.1). The shallowest samples here presented were taken with internal Teflon-coated GO-FLO samplers (see *subsection* 2.2.) as the final sample at about 5 m depth at the end of the complete ~4000 m deep hydrocast. The vertical transit of twice ~4000 m of the open GO-FLO sampler also serves to rinse off any inadvertent contamination before closing the GO-FLO sampler at 5 m depth. The integrity of clean samples is furthermore confirmed by the complete transects of dissolved Fe

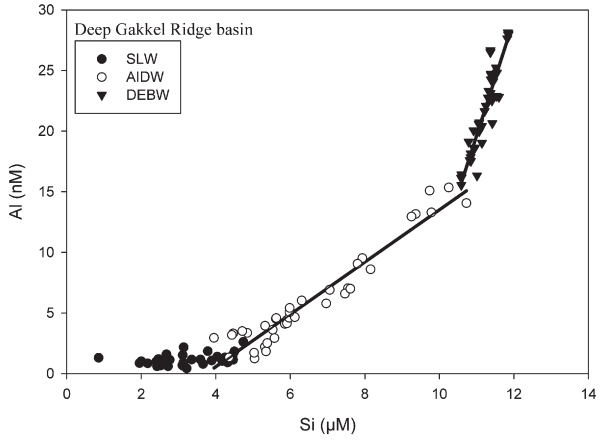

Fig. 18. Concentrations of dissolved aluminium (nM) versus concentrations of dissolved Si (μM) in the deep Gakkel Ridge basin in the Surface Layer Water (SLW) (closed circles), Atlantic and Intermediate Depth Water (AIDW) (open circles) and Deep Eurasian Basin Water (DEBW) (closed triangles). Correlation in Gakkel Ridge AIDW [Al][nM] = 2.2[Si][μM] − 8.0 with $R^2 = 0.93$ $n = 39$ and $P < 0.001$ (Eq. (16)). Correlation in Gakkel Ridge DEBW [Al][nM] = 9.8[Si][μM] − 88.0 with $R^2 = 0.87$ $n = 43$ and $P < 0.001$ (Eq. (17)).

(Klunder et al., 2008) in the same samples as here reported for dissolved Al.

It appears that only a small part of the discrepancy can be explained by the presumed about 10% difference between reactive (unfiltered) Al and dissolved (0.2 μm filtered) Al. Thus it appears this 10% assumption in historic literature is not necessarily justified in surface waters where perhaps a higher than 10% of all Al is in the particulate state. Perhaps seasonal and spatial variations may also exert an influence. Moreover, inadvertent contamination cannot be ruled out either for the historic datasets, notably when sampling was done with Niskin type samplers or by hand instead of using well-flushed GO-FLO samplers.

The here presented general trend of low concentrations of dissolved (0.2 μm filtered) Al in the SML (<1 nM) and subsequently increasing concentrations with depth is more compatible with the observations of Hall and Measures (1998) in 0.4 μm filtered samples (from GO-FLO samplers) at their most northern, deep station in the Nordic Seas. Although the deep concentrations of dissolved Al found in the Arctic (maximum of 28.1 nM) are not as high as the concentrations of around 40 nM reported in the Nordic Seas and Lofoten Basin of the Norwegian Sea (Measures and Edmond, 1992), the similarity in profile shape indicates similar processes may be responsible for the distribution of dissolved Al. This is supported by the observation that there also appears to be a relative enrichment of Al versus Si in the deepest part of the Norwegian Sea compared to the overlying water masses. Measures and Edmond (1992) suggested shelf waters to be the source of the enriched deep water concentrations of Al for the Greenland and Norwegian Sea, by the input of high salinity, high Al, brine waters from the shelf into the deep basins. The brine waters result from the autumn and winter process of sea-ice formation leaving behind the dissolved salts in the ambient seawater.

5.2. Distribution of Al in the Surface Layer Water (SLW)

The concentrations of Al within the SLW (down to 75–150 m depth) in the basins vary between 0.4 nM and 3 nM with an average of 1.3 nM ($n = 124$, S.D. = 0.5). For the uppermost SML (~25 m depth) the concentration of Al varies between 0.4 nM and 1.8 nM with an average value of 0.98 nM ($n = 56$ S.D. = 0.3).

This is different from the concentrations of reactive (unfiltered and not acidified) Al observed by Measures (1999) (see *subsection* 5.1.). Using the highest estimate (0.14 g m^{-2} y^{-1}) of a range (0.033–0.14 g m^{-2} y^{-1}) of aeolian dust input in the Arctic Ocean (Darby et al., 1989), in combination with an Al input model for the temperate Atlantic Ocean (Measures and Brown, 1996), would yield a steady-state concentration of dissolved Al of 1 to 3.5 nM in Arctic Ocean surface waters (Measures, 1999). This is somewhat higher than the average dissolved Al values of 0.98 nM in the SML and 1.3 nM in the SLW here reported. Using the presumed 10% addition for reactive Al in seawater (see *subsection* 5.1.) the total (unfiltered) average values in our samples would be 1.08 nM in the SML and 1.4 nM in the SLW. This still is at or below the above cited input model derived range of 1 to 3.5 nM, thus there is no need to invoke an additional Al input source, i.e. from presumed 'dirty' sea ice, as suggested to explain the much higher concentrations of Al (1.4 to 22.4 nM) in unfiltered seawater reported previously (Measures, 1999). Alternatively latter high values (1.4 to 22.4 nM) may be due to 'dirty' samplers instead. Perhaps for the sea-surface microlayer also collected in the upper 10–20 cm depth sampling (Measures, 1999) an elevated total (unfiltered) Al is not completely inconceivable. Yet for the deeper samples (5–28 m depth) the previously reported 2.4 to 22.2 nM values (Measures, 1999) are inconsistent with our findings.

Gehlen et al. (2003) derived from a global simulation model that an average concentration of Al (dissolved from dust) between 5 and 8 nM should exist in the Arctic Ocean at 25 m depth based on two different dust input scenarios. This range is almost an order of magnitude overestimation compared with the actually measured concentrations of 0.4 to 1.8 nM (average 0.98 nM) in the SML here reported, thus further refinement of the global simulation model is now feasible.

In the Makarov Basin the Al concentrations in the SLW were lower than in the Amundsen Basin and Nansen Basin (see *subsection* 4.4.). On the other hand the concentrations of Si were higher in the SLW of the Makarov basin compared to the SLW of the Nansen Basin and Amundsen Basin. Apparently the Atlantic inflow supplies more Al and less Si to the SLW of the Eurasian Basin than the overall inflow into the Makarov Basin where also a Pacific inflow term has an effect.

The end of transect 5 extends into the shallow Laptev Sea where fluvial input has an important influence due to the outflow of the Lena River. The outflow of the Ob and Yenisey rivers also enters the Laptev Sea (Guay and Falkner, 1997). The freshwater input was evident from lower salinities of 32.6 at 35 m and 29.1 near the surface (see *subsection* 4.6.). However, the concentrations of Al in the Laptev Sea (see *subsection* 4.6.) reached a maximum value of only 2.3 nM at 20 m depth. This indicates that fluvial input is of little influence for the distribution of dissolved Al in the upper water column of the Arctic Ocean, most likely due to effective precipitation of Al in the estuary (Mackin and Aller, 1984; Maring and Duce, 1987; Measures, 1999; Tria et al., 2007 and references therein).

5.3. Sources for Al and Si in intermediate and deep waters

The distributions of both Al and Si within the intermediate waters (AIDW comprising ALW and IDW) and the deep basins (DEBW comprising EBDW and EBBW; and DMBW) may offer some clues to their sources. These sources can be either by water mass transport and mixing, or by (regional) biogeochemical processes. Lateral transport and mixing of water masses from elsewhere may come from (i) the Atlantic Ocean or (ii) the Pacific Ocean, or (iii) from downward convection of waters from the extensive Arctic shelf seas. Biogeochemical processes may be either (iv) dissolution (*in situ* or elsewhere) of diatom frustules comprising both Si and trace amounts of Al, or (v) *in situ* dissolution from sediment sources with likely higher Al to Si element ratio composition.

Below we will argue that the intermediate layer waters (AILW) are influenced by different source waters from either Atlantic or Pacific origin with most likely some additional dissolution of diatom frustules. For the deepest Eurasian Basin waters (DEBW) we will argue that there is no more direct influence of Atlantic waters, in fact we attribute the high Al: Si ratio to downward convection of waters from the extensive Arctic shelf seas. In the deepest Makarov Basin waters (DMBW) its classical Pacific source term via the Canadian Basin flowing over the Mendeleyev Ridge must be complemented by overflow across the Lomonosov Ridge of Eurasian Basin water with lower Si yet higher Al than the Pacific source waters.

5.4. Distribution of Al in the Atlantic and Intermediate Depth Water (AIDW)

When looking at the AIDW, it appears that the Nansen and Amundsen Basins had significantly similar regression slopes of the Al–Si relation. In the Makarov Basin however, the slope of the Al–Si relation is significantly less steep in the same water layer (Table 3); i.e. there is relatively less Al and more Si in the AIDW of the Makarov Basin compared to the AIDW of the Eurasian Basin. The difference between the AIDW of the Eurasian Basin and the AIDW of the Makarov Basin is most likely caused by the different origins of the water in the different basins (see Section 3.). The data here presented show less Si and more Al are supplied to the AIDW of the Eurasian Basin by the Atlantic inflow, whilst comparably more Si and less Al are supplied to the AIDW of the Makarov Basin by the Pacific inflow (Figs. 10 and 11). The relatively stronger influence of the warm Atlantic inflow on

the ALW of the Eurasian Basin is also visible in the higher potential temperature of the ALW in the Eurasian Basin compared to the ALW in the Makarov Basin (Fig. 9). Despite these differences, a strong correlation is found between Si and Al in the AIDW of all three basins (Table 3). This indicates that mixing of the different water sources is not the only process controlling the distributions of Al and Si in the AIDW, i.e. local dissolution of biogenic matter (e.g. diatom frustules) also plays a role in the AIDW.

Both Al and Si are nearly depleted in the SML and concentrations increase with depth in the water column. The strong correlation between Al and Si points towards the coupling between the biogeochemistries of Al and Si, as suggested by various authors (e.g. Chou and Wollast, 1997; Hydes et al., 1988; Kramer et al., 2004; Mackenzie et al., 1978; Stoffyn, 1979). As described in detail by Gehlen et al. (2002), the Al is incorporated in the siliceous frustules of living diatoms in the photic surface layer. Upon senescence of a diatom bloom and/or grazing, the heavy opaline frustules settle down into deeper waters. When the biogenic silica is degraded and dissolves throughout the water column, the incorporated Al is released as well. Based on the observed correlations, at least part of the released Al stays in the soluble fraction, possibly aided by the pressure-dependent solubility of Al (Moore and Millward, 1984). If there is a strong contribution of Al dissolution from biogenic silica, this implies that the Al/Si ratio observed in diatom frustules is reflected in the Al/Si ratio represented in the slope of the Al–Si relation (Kramer et al. 2004). To our best knowledge there are no data available on the Al/Si ratio in Arctic diatom frustules. The Al/Si ratio worldwide ranges from $0.033*10^{-3}$ to $0.6*10^{-3}$ in Antarctic diatom samples (Collier and Edmond, 1984; Van Bennekom et al. 1991), to $11*10^{-3}$ in biogenic silica in marine sediment samples (Van Beusekom et al. 1997). The samples of biogenic silica from marine sediments are most likely contaminated by Al from other sediment particles, i.e. show a too high Al:Si ratio to be representative of pure diatom frustules. Gehlen et al. (2002) found ratios ranging from $0.07*10^{-3}$ to $8.3*10^{-3}$ in diatom cultures and natural diatom samples.

The overall Al/Si ratio in the Arctic Ocean, from the slopes of the Al–Si relation, in the AIDW of the Nansen and Amundsen Basins of all transects combined is:

$$[\mathrm{Al}][\mathrm{nM}] = 2.2[\mathrm{Si}][\mu\mathrm{M}] - 7.7 \quad (R^2 = 0.92 \text{ and } n = 193) \tag{18}$$

The Al/Si ratio of $2.2*10^{-3}$ is quite similar to the value of about $2.0*10^{-3}$ that was found in the AIDW of the Makarov Basin (Eqs. (11), (12) and (13); Table 3). These ratios are within the range of ratios found by Gehlen et al. (2002), and 3 to 4 times higher than the highest Al/Si ratio found in Antarctic diatom samples, but much lower than the ratio found in biogenic silica in marine sediments. The ratio value of about $2.2*10^{-3}$ in the AIDW is also much lower than the Al/Si regression slopes found in the water column of the eastern Mediterranean Sea, the western Mediterranean Sea and the surface water of Canary Basin, $10*10^{-3}$, $11*10^{-3}$ and $40*10^{-3}$, respectively (Hydes et al., 1988; Chou and Wollast, 1997; Kramer et al., 2004). Apparently, the relationship between Al and Si is highly variable between different seas and oceans. Moreover in other oceans like the North Pacific Ocean and the Southern Ocean such Al–Si relationship does not exist at all (e.g. Orians and Bruland, 1986; Middag et al., 2009).

Not all dissolved Al and Si in the water column will be from biogenic silica as there is also input of terrestrial alumino–silicates via the atmosphere, sea ice or rivers. These alumino–silicates originate from the continental crust and have a much higher Al/Si ratio of about 1:3 (Taylor, 1964; Wedepohl, 1995) than the average ratio of about 1:400 observed in biogenic silica (Gehlen et al., 2002 and references therein) when excluding the highest and lowest values. Even modest dissolution of terrestrial alumino-silicates would already lead to a significant increase in the dissolved Al/Si ratio. Depending on the Al/Si ratio of biogenic silica in the Arctic Ocean and the influence of terrestrial alumino-silicates input, the observed Al–Si ratio can largely be explained by the dissolution of Al and Si from biogenic silica.

Based on the strong correlation between Al and Si and the low dissolved Al/Si ratio, it appears that biogenic silica is the most important factor controlling the distribution of these elements in the AIDW of the Arctic Ocean. The particle-reactive nature of Al would explain the low surface concentrations of Al regardless of the source of Al. However, unless the majority of the Al is scavenged onto biogenic siliceous particles, the strong correlation between Al and Si remains unexplained. Overall, the nutrient-like profile of Al, the strong correlation with Si and the consistency between the dissolved Al/Si ratio reported here and the biogenic Al/Si ratio elsewhere reported does indicate a strong (biological) influence of biogenic silica on the Al distribution through the incorporation of Al in biogenic silica and/or preferential scavenging of Al onto biogenic siliceous particles. Unfortunately, it is not possible to distinguish between the relative importances of incorporating Al in biogenic silica versus preferential scavenging onto biogenic siliceous particles based on the data presented here. Laboratory or *in situ* studies into Al uptake by diatoms and kinetics of Al binding to biogenic siliceous and other particles could provide more insight into the processes.

5.5. Distribution of Al in the deep basins

In the deep Eurasian Basin two distinct trends can be discerned. Approaching the continental slope on the Eurasian side of the basins the concentrations of Al were elevated relative to the same depths in the central basin. Furthermore, there is a relative enrichment of Al to Si in the DEBW compared to the AIDW, evident as a steeper slope of the Al–Si relationship. These steeper slopes between $7.4*10^{-3}$ and $13.5*10^{-3}$ (Table 4) are akin to the Al/Si regression slopes found in the water column of the eastern and western Mediterranean Sea, $10*10^{-3}$ and $11*10^{-3}$ respectively. Such enrichment of Al is absent in the deep Makarov Basin where the deep concentrations of Al are lower and the concentrations of Si are higher than in the Eurasian Basin. Moreover, the concentrations of Si decrease below 2500 m depth in the Makarov Basin, which is not the case in the Eurasian Basin (see *subsection* 4.4.). The concentrations of Al, on the other hand, continuously increased with depth below 2500 in the Makarov Basin, but this increase was less steep than in the Eurasian Basin as the concentrations of Al did not increase over a maximum 19 nM value in the deep layers (see *subsection* 4.4. and 4.5.).

Upward vertical diffusion of Al from *in situ* dissolution from the deepest bottom sediments (Hydes, 1977) appears not to be of significant influence in the Eurasian Basin as the highest concentrations are usually found just below the potential temperature minimum which are still several hundreds of metres above the bottom sediments (Figs. 7 and 12). For the same reasons pressure-dependent solubility of Al–containing clays (Moore and Millward, 1984) appears to be an unsatisfactory explanation.

The Atlantic water entering the Arctic Ocean has more influence on the Eurasian Basin than on the Makarov Basin (see *subsection* 5.2. and 5.4.). However, it appears unlikely that this is solely responsible for the basin-wide higher concentrations in the deep Nansen Basin and Amundsen Basin compared to the deep Makarov basin. The Atlantic influences mostly the AIDW but this effect fades away with distance into the basin away from the Atlantic Ocean. Furthermore, at greater depths in the AIDW complex the Atlantic signal of potential temperature and salinity from the upper ALW quickly fades away into the lower Intermediate Depth Water. Moreover, in the deepest water of the Nansen Basin and Amundsen Basin the potential temperature (Fig. 9) was lower than that of water at the same depth in the Makarov Basin. This lower potential temperature in the deepest Nansen and Amundsen Basins cannot be caused by inflow of Atlantic water, because that is actually warmer instead of colder.

The dissolution of diatom frustules appears not to be the main factor controlling the distribution of Al and Si in the deepest part of the basins, even though strong correlations are found in the deep Eurasian Basin. However, dissolution of diatom frustules alone cannot account for the observed Al maximum several hundreds of metres above the bottom sediments in the Eurasian Basin (Fig. 7).

Furthermore, in the deep Makarov Basin the correlation between Al and Si completely disappears as the concentrations of Si start to decrease below 2500 m (Fig. 13c). Apparently, the distributions of Al and Si in the deep basins and the differences between the deep Eurasian Basin and the deep Makarov Basin cannot be explained by the inflow of Atlantic water, the inflow from Pacific water, the dissolution of diatom frustules or the *in situ* dissolution from the bottom sediments. Therefore, the downward convection of waters from the extensive Arctic shelf seas has to be taken into account to explain the distribution of Al and Si in the deep Arctic Ocean. This is consistent with what is known about the hydrography of the region as will be described below. Furthermore, the concentrations of Barium from the same cruise were also relatively enriched in the DEBW, indicative of shelf water input (Roeske et al., in preparation).

The literature reveals that sea-ice formation, brine rejection and subsequent dense water formation in the Barents and Kara Seas leads to convection down the slopes of the Eurasian Basin (Rudels et al. 2000, Rusakov et al. 2004). This dense, shelf-derived water delivers terrigenous particulate matter, rich in Al (Rusakov et al. 2004), into the Nansen Basin and Amundsen Basin. When dense shelf-derived water cascades down the continental slope into the basins it mixes with the boundary current (Rudels et al. 2000) and possibly picks up sediment as suggested by Moran and Moore (1991). The partial dissolution of this resuspended sediment could be an additional source of Al for the deep water. According to Rudels et al. (2000) the deepest (bottom) water layer in the Eurasian Basin receives most input from slope convection from the Severnaya Zemlya area. The Barents Sea on the other hand, exerts the biggest influence on the deep water above the bottom layer. The slope convection from Severnaya Zemlya entrains more relatively warm boundary current water causing the deepest (bottom) water layer to be slightly warmer, hence the observed potential temperature minimum in the Eurasian Basin. The maximum concentrations of Al in the Amundsen Basin and Nansen Basin generally being found just at or slightly below the potential temperature minimum (Fig. 12) could be explained by the difference in the two deep water sources. Assume for the sake of argument, the Barents Sea supplies more Al-rich particles that tend to sink to the deeper parts of the water mass and dissolve with time and/or depth. In this case most dissolved Al will be found in the deepest part of the water mass supplied by the Barents Sea. Mixing with the underlying water from the Severnaya Zemlya region that (hypothetically) contains less Al and further sinking of dissolving Al-rich particles could explain the dissolved Al maximum just below the potential temperature minimum. However, in the middle of the Nansen Basin in transect 3, the maximum Al values did not correspond with the potential temperature minimum indicating that the theory does not completely explain the deep Al distribution.

Unfortunately, the deep water column was sampled with relatively low resolution, compared to the upper water column, rendering a more quantitative approach impossible for deep waters. Looking at the general Al distribution in the DEBW, the highest Al values are found in the Nansen Basin and the concentrations decrease with distance from the continental slope, into the deeper Amundsen Basin (Fig. 10). This trend is an indication that the source of the extra Al is from the continental slope. Furthermore, the steepest slopes for the Al–Si relation in the DEBW were found in the Nansen Basin, in transects 2 and 3 (Table 4). Thus apparently, the strongest influence on the Al enrichment is in this region, closest to the Saint Anna Trough. This trough is an important source for the inflow of dense shelf-derived water, containing Al-rich particulate matter, into the Eurasian Basin (Rudels et al. 2000). Unfortunately the formation of the dense water at the shelf due to ice formation and brine rejection and subsequent down-flow of this dense shelf-derived water by slope convection occurs in winter. Since the data here presented was collected in summer no direct observations and measurements of this water mass could be made to confirm our concept.

The dissolved Al/Si ratio from the slope of the Al–Si relation in the Barents Sea was $1.2*10^{-3}$ and $3.3*10^{-3}$ in transect 1 and transect 2, respectively (Table 2). Input into the DEBW of shelf water with these dissolved ratios cannot account for the increased dissolved Al/Si ratios in the DEBW compared to the AIDW. However, according to Rusakov et al. (2004), this shelf-derived water has a high particle load (up to 1.2 mg L^{-1}) with about 7.6% terrigenous matter by weight. The DEBW on the other hand has low particle concentrations, typical for deep ocean water. The particle concentration of the dense shelf-derived water gets strongly diluted by mixing with the low particle DEBW. A lower particle concentration means a lower scavenging rate for Al which aids the dissolution of Al from the (terrigenous) particles, in addition to the presumed pressure-dependent solubility. Terrigenous matter has a high Al:Si ratio of about 1:3 (see *subsection* 5.4.) and dissolution of this terrigenous matter in the shelf water that cascades down the slope would increase the dissolved Al:Si ratio of the DEBW. The AIDW in the Eurasian Basin has an average Al:Si ratio (from the slope of the Al–Si relation) of 1:450 and the DEBW has an average Al:Si ratio of 1:100. If we assume that the shelf-derived water carries the terrigenous signature in the Al:Si ratio due to dissolving terrigenous matter, this ratio will be about to 1:3. For example solving the simple equation:

$$(\text{Al : Si DEBW}) = x(\text{Al : Si AIDW}) + (1-x)(\text{Al : Si Terrigenous matter}) \quad (19)$$

gives $x = 0.98$. This means that 98% water with an Al:Si ratio as observed in the AIDW after mixing with only 2% water with an Al:Si ratio of terrigenous matter results in water with the actual Al:Si ratio as observed in the DEBW (Table 4).

In the water column of the Makarov Basin a Si maximum at about 2500 m was observed (see *subsection* 4.4. and 4.5.). The origin of this deep Si maximum was suggested by Swift et al. (1997) to be Canada Basin water flowing in over the 2500 m sill of the Mendeleyev Ridge. The higher Si values deeper than 2500 m depth in the Makarov Basin compared to the Eurasian Basin (see above) appear to be caused by this inflow. The continued increase in concentrations of Al with increasing depth in contrast to the decreasing Si values in the deepest water layers indicate that the Canada Basin inflow mixes with water of lower concentrations of Si but higher concentrations of Al which is consistent with the water from the deep Eurasian Basin. Therefore, the deep Makarov Basin is not only influenced by the water flowing in over the Mendeleyev sill, but most likely also by water flowing in over the Lomonosov Ridge from the Eurasian Basin. This strengthens the ideas of Jones et al. (1995) of inflow from the Eurasian Basin into the Makarov Basin. However, this expected inflow of water was not observed by Björk et al. (2007). The relative influence of the different water masses on the deep Makarov Basin remains debatable, but the distributions of Al and Si here presented indicate the deep Makarov Basin is influenced by inflow over the Lomonosov Ridge of Eurasian Basin water.

Overall, the different sources of the deep waters appear to be the reason for the higher Al and lower Si values in the deep Eurasian Basin compared to the deep Makarov Basin.

6. Conclusions

The general background concentration of Al observed in the SML of the Arctic Ocean was sub-nanomolar. Therefore, no significant influence from either dust input, or 'dirty' sea ice is evident. In all three basins the Al shows a nutrient-like profile and a very strong

correlation with Si. The Al distribution in the SLW and AIDW can partly be explained by the different origins of the waters influencing these layers. Atlantic water is relatively rich in Al and poor in Si and has the most influence on the Eurasian Basin. Pacific water, on the other hand, is relatively poor in Al and rich in Si and has the biggest influence on the Makarov Basin. Therefore, the concentrations of Al in the SLW were lowest in the Makarov Basin and higher in the Eurasian Basin. Moreover, the Al/Si ratio derived from the slope of the Al–Si relation in the AIDW, was lower in the Makarov Basin compared to the Eurasian Basin. Very little direct influence of fluvial input is observed with only minor elevations in Al, up to 2.3 nM, in the Laptev Sea.

The Al/Si ratio derived from the slope of the Al–Si relation in the intermediate water can, at least partly, be explained by the dissolution of biogenic silica. This depends, however, on the Al/Si ratio assumed for biogenic silica, for which a large range is found in the literature. Nevertheless, there appears to be a strong biological influence on the cycling and distribution of Al in the Arctic Ocean through the formation and dissolution of biogenic silica.

In the deep Eurasian Basin there is a relative enrichment of Al with respect to Si in the DEBW compared to the overlying AIDW. In the Makarov Basin this relative enrichment is absent. The relative enrichment of Al with respect to Si in the deep Eurasian Basin's DEBW compared to the AIDW appears to be caused by downward flow from the Barents and Kara Seas of dense shelf-derived water containing Al-rich particulate matter. This is clearly visible in the maximum Al values in the deep Eurasian Basin that were generally observed just below the potential temperature minimum and there was a trend of higher Al values towards the continental slope. Furthermore, the highest Al values and steepest slopes of the Al–Si relation were observed near the St Anna Trough which is an important source for the inflow of dense shelf-derived water into the Eurasian Basin (Rudels et al. 2000). The source of the Al enrichment is most likely a combination of partial dissolution of the Al content of the terrigenous particulate matter in the dense shelf-derived water itself and partial dissolution of Al from resuspended terrigenous sediment from the continental slope. Both sources could be intensified by the pressure-dependent solubility of Al.

The deep Makarov Basin appears to be influenced by both Canada Basin water flowing in over the Mendeleyev Ridge and Eurasian Basin water flowing in over the Lomonosov Ridge. This is found in the Si and Al distributions in the deep Makarov Basin. The concentrations of Si decreased below the Si maximum at 2500 m in the Makarov Basin while the deep concentrations of Al continuously increased with depth. Furthermore, the deep Makarov Basin has higher concentrations of Si and higher potential temperatures but lower concentrations of Al than the deep Eurasian Basin. The mixing of relatively Si-rich Canada Basin water with relatively Al-rich Eurasian Basin water explains the observed Al and Si distributions. This supports the concepts of Jones et al. (1995).

Acknowledgements

The authors are most grateful to the master S. Schwarze, officers and crew of R.V. Polarstern for their splendid support during the expedition. Special thanks to Sven Ober and Lorendz Boom for the operation of the all-titanium CTD sampling system, Loes Gerringa for her constructive comments and my colleagues Maarten Klunder and Charles-Edouard Thuróczy for their help with sampling and general support. Last but not least many thanks to all participants of expedition ARK XXII/2 for their help and support and for making the long expedition enjoyable. This work was funded by The Netherlands Organisation for Scientific Research, IPY-NL-GEOTRACES sub-project: 851.40.101. Constructive comments of two anonymous reviewers and the associate editor are appreciated and have led to significant improvements of the manuscript.

References

Aguilar-Islas, A.M., Resing, J.A., Bruland, K.W., 2006. Catalytically enhanced spectrophotometric determination of manganese in seawater by flow-injection analysis with a commercially available resin for on-line preconcentration. Limnology and Oceanography Methods 4, 105–113.

Anderson, L.G., Björk, G., Holby, O., Jones, E.P., Kattner, G., Koltermann, K.P., Liljeblad, B., Lindegren, R., Rudels, B., Swift, J.H., 1994. Water masses and circulation in the Eurasian Basin: results from the Oden 91 expedition. Journal of Geophysical Research, Oceans 99 (C2), 3273–3283.

Aoyama, et al., 2008. 2006 Inter-comparison Study for Reference Material for Nutrients in Seawater. Technical reports of the Meteorological Research Institute No. 58. ISSN 0386-4049.

Björk, G., Jakobsson, M., Rudels, B., Swift, J., Anderson, L., Darby, D., Backman, J., Coakley, B., Winsor, P., Polyaki, L., Edwards, M., 2007. Bathymetry and deep-water exchange across the central Lomonosov Ridge at 88–89 N. Deep-Sea Research 54 (8), 1197–1208.

Broecker, W.S., Peng, T.H., 1982. Tracers in the Sea. Eldigio Press, New York. p. 689.

Brown, M.T., Bruland, K.W., 2008. An improved flow-injection analysis method for the determination of dissolved aluminum in seawater. Limnology and Oceanography Methods 6, 87–95.

Bruland, K.W., Franks, R.P., Knauer, G.A., Martin, J.H., 1979. Sampling and analytical methods for the determination of copper, cadmium, zinc, and nickel at the nanogram per liter level in sea water. Analytica Chimica Acta 105 (1), 233–245.

Chou, L., Wollast, R., 1997. Biogeochemical behavior and mass balance of dissolved aluminium in the western Mediterranean Sea. Deep-Sea Research II 44 (3–4), 741–768.

Collier, R., Edmond, J., 1984. The trace element geochemistry of marine biogenic particulate matter. Progress in Oceanography 13 (2), 113–199.

Darby, D.A., Naidu, A.S., Mowatt, T.C., Jones, G., 1989. Sediment composition and sedimentary processes in the Arctic Ocean. In: Hermann, Y. (Ed.), The Arctic Seas. Van Nostrand-Reinhold, New York. 888 pp.

De Baar, H.J.W., Timmermans, K.R., Laan, P., de Porto, H.H., Ober, S., Blom, J.J., Bakker, M.C., Schilling, J., Sarthou, G., Smit, M.G., Klunder, M., 2008. Titan: a new facility for ultra-clean sampling of trace elements and isotopes in the deep oceans in the international Geotraces program. Marine Chemistry 111 (1–2), 4–21.

Gehlen, M., Beck, L., Calas, G., Flank, A.M., Van Bennekom, A.J., Van Beusekom, J.E.E., 2002. Unraveling the atomic structure of biogenic silica: evidence of the structural association of Al and Si in diatom frustules. Geochimica et Cosmochimica Acta 66 (9), 1604–1609.

Gehlen, M., Heinze, C., Maier-Reimer, E., Measures, C.I., 2003. Coupled Al–Si geochemistry in an ocean general circulation model: a tool for the validation of oceanic dust deposition fields? Global Biogeochemical Cycles 17 (1), 1028.

GEOTRACES Planning Group, 2006. GEOTRACES Science Plan. Scientific Committee on Oceanic Research, Baltimore, Maryland.

Grasshoff, K., Erhardt, M., Kremling, K., 1983. Methods of seawater analysis. Verlag Chemie, Weinheim, Germany. 419 pp.

Guay, C., Falkner, K., 1997. Barium as a tracer of Arctic halocline and river waters. Deep-Sea Research II 44 (8), 1543–1569.

Hall, I.R., Measures, C.I., 1998. The distribution of Al in the IOC stations of the North Atlantic and Norwegian Sea between 52° and 65° North. Marine Chemistry 61 (1–2), 69–85.

Han, Q., Moore, J.K., Zender, C., Measures, C., Hydes, D., 2008. Constraining oceanic dust deposition using surface ocean dissolved Al. Global Biogeochemical Cycles 22 (2), GB2003.

Hydes, D.J., 1977. Dissolved aluminium in sea water. Nature 268 (5616), 136–137.

Hydes, D.J., 1983. Distribution of Al in waters of the North East Atlantic 25 degr. N to 35 degr. N. Geochimica et Cosmochimica Acta 47 (5), 967–973.

Hydes, D.J., de Lange, G.J., de Baar, H.J.W., 1988. Dissolved aluminum in the Mediterranean. Geochimica et Cosmochimica Acta 52 (8), 2107–2114.

Johnson, K.S., Boyle, E., Bruland, K., Measures, C., Moffett, J., Aquilarislas, A., Barbeau, K., Cai, Y., Chase, Z., Cullen, J., Doi, T., Elrod, V., Fitzwater, S., Gordon, M., King, A., Laan, P., Laglera-Baquer, L., Landing, W., Lohan, M., Mendez, J., Milne, A., Obata, H., Ossiander, L., Plant, J., Sarthou, G., Sedwick, P., Smith, G.J., Sohst, B., Tanner, S., Van Den Berg, S., Wu, J., 2007. Developing standards for dissolved iron in seawater. Eos, Transport of American Geophys. Union 88 (11), 131–132.

Jones, E.P., Rudels, B., Anderson, L.G., 1995. Deep waters of the Arctic Ocean: origins and circulation. Deep-Sea Research 42 (5), 737–760.

Klunder, M.B., de Baar, H.J.W., Laan, P., Bakker, K., Ober, S., Rutgers van der Loeff, M., 2008. IPY-Geotraces: sources and distribution of dissolved iron in the Arctic Ocean. SCAR Open Science Conference St Petersburg 2008.

Kramer, J., Laan, P., Sarthou, G., Timmermans, K.R., de Baar, H.J.W., 2004. Distribution of dissolved aluminium in the high atmospheric input region of the subtropical waters of the North Atlantic Ocean. Marine Chemistry 88 (3–4), 85–101.

Mackenzie, F.T., Stoffyn, M., Wollast, R., 1978. Aluminum in seawater: control by biological activity. Science 199 (4329), 680–682.

Mackin, J.E., Aller, R.C., 1984. Processes affecting the behavior of dissolved aluminum in estuarine waters. Marine Chemistry 14 (3), 213–232.

Maring, H.B., Duce, R.A., 1987. The impact of atmospheric aerosols on trace metal chemistry in open ocean surface seawater, 1, Aluminum. Earth and Planetary Science Letters 84 (4), 381–392.

Measures, C.I., 1999. The role of entrained sediments in sea ice in the distribution of aluminium and iron in the surface waters of the Arctic Ocean. Marine Chemistry 68 (1–2), 59–70.

Measures, C.I., Edmond, J.M., 1990. Aluminum in the South-Atlantic—steady-state distribution of a short residence time element. Journal of Geophysical Research, Oceans 95 (C4), 5331–5340.

Measures, C.I., Edmond, J.M., 1992. The distribution of aluminium in the Greenland Sea and its relationship to ventilation processes. Journal of Geophysical Research, Oceans 97 (C11), 17787–17800.
Measures, C.I., Brown, E.T., 1996. Estimating dust input to the Atlantic Ocean using surface water Al concentrations. In: Guerzoni, Chester (Ed.), The Impact of African Dust Acrossthe Mediterranean. Kluwer. 389 pp.
Measures, C.I., Vink, S., 2000. On the use of dissolved aluminium in surface waters to estimate dust deposition to the ocean. Global Biogeochemical Cycles 14 (1), 317–327.
Middag, R., van Slooten, C., de Baar, H.J.W., de Laan, P., 2009. Dissolved aluminium in the Southern Ocean. Deep Sea Research II 115 (4–5), 176–195.
Moore, R.M., 1981. Oceanographic distributions of zinc, cadmium, copper and aluminium in waters of the central Arctic. Geochimica et Cosmochimica Acta 45 (12), 2475–2482.
Moore, R.M., Millward, G.E., 1984. Dissolved-particulate interactions of aluminium in ocean water. Geochimica et Cosmochimica Acta 48 (2), 235–241.
Moran, S.B., Moore, R.M., 1991. The potential source of dissolved aluminium from resuspended sediments to the North Atlantic Deep Water. Geochimica et Cosmochimica Acta 55 (10), 2745–2751.
Orians, K.J., Bruland, K.W., 1985. Dissolved aluminum in the Central North Pacific. Nature 316 (6027), 427–429.
Orians, K.J., Bruland, K.W., 1986. The biogeochemistry of aluminum in the Pacific-Ocean. Earth and Planetary Science Letters 78 (4), 397–410.
Resing, J., Measures, C.I., 1994. Fluorimetric determination of Al in seawater by FIA with in-line preconcentration. Analytical Chemistry 66 (22), 4105–4111.
Rudels, B., Muench, R.D., Gunn, J., Schauer, U., Friedrich, H.J., 2000. Evolution of the Arctic Ocean boundary current north of the Siberian Shelves. Journal of Marine Systems 25 (1), 77–99.
Rusakov, V.YU., Lisitsyn, A.P., Izotova, S.S., Moskalev, A.S., Gazenko, A.O., Rahold, F., 2004. Distribution and mineral composition of particulate matter in the Franz Victoria Trough (Northern Barents Sea). Oceanology 44 (2), 247–256 Translated from Okeanologiya 44 (2), 267–277.
Schauer, U. (Ed.), 2008. The Expedition ARKTIS-XXII/2 of the research vessel "Polarstern" in 2007: Berichte zur Polar- und Meeresforschung 579. 265 pp.
Stoffyn, M., 1979. Biological control of aluminium in seawater: experimental evidence. Science 203 (4381), 651–653.
Stoffyn, M., Mackenzie, F.T., 1982. Fate of dissolved aluminum in the oceans. Marine Chemistry 11 (2), 105–127.
Swift, J.H., Jones, E.P., Carmack, E.C., Hingston, M., Macdonald, R.W., McLaughlin, F.A., Perkin, R.G., 1997. Waters of the Makarov and Canada Basins. Deep-Sea Research II 44 (8), 1503–1529.
Taylor, S.R., 1964. Abundance of chemical elements in the continental crust: a new table. Geochimica et Cosmochimica Acta 28 (8), 1273–1285.
Tria, J., Butler, E.C.V., Haddad, P.R., Bowie, A.R., 2007. Determination of aluminium in natural water samples. Analytica Chimica Acta 588 (2), 153–165.
Van Bennekom, A.J., Jansen, F., Van Der Gaast, S., Van Iperen, J., Pieters, J., 1989. Aluminum-rich opal: an intermediate in the preservation of biogenic silica in the Zaire (Congo) deep-sea fan. Deep-Sea Research Part A 36 (2), 173–190.
Van Bennekom, A.J., Buma, A.G.J., Nolting, R.F., 1991. Dissolved aluminium in the Weddell-Scotia confluence and effect of Al on the dissolution kinetics of biogenic silica. Marine Chemistry 35 (1–4), 423–434.
Van Beusekom, J.E.E., Weber, A., 1992. Decreasing diatom abundance in the North Sea: the possible significance of aluminium. In: Colombo, G., et al. (Ed.), Marine Eutrophication and Population Dynamics. Olsen and Olsen, Fredensborg, Denmark, pp. 121–127.
Van Beusekom, J.E.E., van Bennekom, A.J., Tréguer, P., Morvan, J., 1997. Aluminium and silicic acid in water and sediments of the Enderby and Crozet Basins. Deep-Sea Research II 44 (5), 987–1003.
Wedepohl, K.H., 1995. The composition of the continental crust. Geochimica et Cosmochimica Acta 59 (7), 1217–1232.
Zar, J.R., Biostatistical analysis. 4th ed. New Jersey: Prentice-Hall, Inc.; 1999.